Research Article

Cyanobacterial Biomass Estimation in Subtropical and Temperate Reservoirs by Sentinel-2

Xavier Sòria-Perpinyà[1], Juan Soria[2], María Dolores Sendra[2], Viviane Moschini-Carlos[3], Rebeca Pérez González[2], Esther Patricia Urrego[1], Jesús Delegido[1], Eduardo Vicente[2], Marcelo Pompêo[4], José Moreno[1]

1. Image Processing Laboratory, Universitat de València; 2. Cavanilles Institute of Biodiversity and Evolutionary Biology (ICBiBE), Universitat de València; 3. Instituto de Ciência e Tecnologia, Universidade Estadual Paulista, Brazil; 4. Institute of Biosciences, Department of Ecology, Universidade de São Paulo, Brazil

The study of cyanobacterial biovolume, the relative abundance of phytoplankton in terms of biomass, using remote sensing is not common. Its estimation can be done in two ways, indirectly through the determination of the phycocyanin concentration, since it is their main pigment, or directly by determining their abundance or biovolume. This work aims to improve the expertise for the cyanobacterial biovolume directly estimation with Sentinel-2 imagery. To develop the algorithm empirically 43 georeferenced samples were collected, 20 from the sub-tropical zone and 23 from the temperate zone, which cyanobacterial biovolumes were determined. Images were resampled, atmospherically corrected with the Case2 eXtreme neuronal net and the remote sensing reflectance were extracted. The best results were retrieved with the NDB5B4, obtaining: R^2 of 0.92, RMSE of 1.71 $mm^3\ L^{-1}$ and NRMSE of 7.6%. To demonstrate its consistency and functionality, the algorithm was applied to images thorough two years, to reproduce both temporal and spatial variations of the cyanobacterial biomass. The highest values were recorded in the subtropical zone. A tail-dam asymmetry was observed in both climatic zones. In the temperate zone, the annual variation registered a minimum and a maximum annual value, while more variations were registered in the subtropical zone.

Corresponding author: Xavier Sòria-Perpinyà, javier.soria-perpina@uv.es

Introduction

Cyanobacteria play a crucial role in the aquatic environment since they are directly involved in essential processes of the ecosystems like the carbon and nitrogen cycles[1]. However, freshwater resources are under a variety of threats, including climate change, environmental degradation, increased demands and cultural eutrophication that will further reduce water quality and quantity[2] considering population growth as direct effects (increase in demand and wastewater), and those derived from climate change as in-direct effects (decrease in precipitation, increase in

 doi.org/10.32388/IEUZZR

temperature, evaporation and retention time). Some specific effects –e.g., anthropogenic nutrient loading, enhanced vertical stratification, increased residence time, rising temperatures, increasing frequencies and magnitudes of extreme weather events[3], and alterations in land-use practices, such as urbanisation or agricultural practices[4]– may favour, influence and promote changes in the phytoplankton community and the cyanobacterial growth.

The dominance of cyanobacteria in the total algal population was associated with higher phosphorus concentrations and low nitrogen concentrations[5], as they are able to fix dissolved dinitrogen gas into organic nitrogen[6] and store excess nutrients like phosphorus[7]. Other adaptations such as low light requirements[8][9], increased growth rates at higher temperatures[10][11] and buoyancy regulation mechanisms[12] further al-low cyanobacteria to prosper in warmer and nutrient enriched waters[13]. As a consequence, harmful algal blooms (HABs) now occur at a higher frequency, intensity and du-ration than previously recorded, increasing the risk of human contact with toxic cyano-bacteria[14][15]. HABs are associated with proliferation of cyanotoxins, food web altering, hypoxia[16][17], human respiratory irritation, taste and odour of potable water, human illness as a result of ingestion or skin exposure during recreational activities[18], death of pets, domestic animals, and wildlife[19], undesirable finished drinking water, increased drinking water treatment costs, and economic and infrastructure costs such as loss of revenue from recreational systems and from businesses that rely on potable water[20][21].

For these reasons, in 1999 the World Health Organization formulated some recommendations at an international level for the health monitoring of cyanobacteria in waters for bathing and drinking purposes[16][22], establishing vigilance and alert levels for drinking water and guidance levels for bathing waters, corresponding to abundance and biovolume values. These levels are especially important in reservoirs subject to eutrophication because they can develop major cyanobacterial blooms when they warm and undergo thermal stratification during the summer months of each year[23]. This problem, although already present in some temperate reservoirs, could become the norm like in tropical reservoirs in the near future. According to Amorim et al.[24], given the predictions of increased eutrophication, warming and salinization of waters, cyanobacterial blooms expected to become more intense in tropical reservoirs.

Given the risk that cyanobacteria pose to aquatic ecosystems, including drinking water reservoirs, it is necessary to develop tools to accurately estimate cyanobacterial biovolume both within and across water bodies[25]. While field sampling is certainly necessary and will continue to be so, managers need other options to improve monitoring, reduce costs, and minimise potential exposures associated with sample collection[18]. Satellite remote sensing can complement field sampling by providing regular, synoptic coverage of algal and cyanobacterial abundance for regional monitoring at resolutions unattainable by field sampling[26][27]. This is an essential tool for water bodies monitoring as an assessing or warning method, which helps to obtain higher temporal and spatial resolution data[28][29].

Studying cyanobacteria biovolume using remote sensing is not common, but why use biovolume? It's a fact that without a correct knowledge of the phytoplankton community it is not possible to have an accurate comprehension of the aquatic ecosystems. Phytoplankton is characterised by its great variability in cell size among different genera and even between different individuals. Actually, there is a wide range of orders in magnitude for cell biovolume of phytoplankton[30]. This is precisely why phytoplankton biovolume is traditionally calculated to estimate the relative abundance of each phytoplankton taxa in terms of biomass instead of cell counts. Other conventional biomass-related parameters, such as chlorophyll a concentration (Chl_a), are known to vary dramatically with environmental conditions, such as light and nutrient availability[31]. On the other hand, regarding the relationship of the Chl_a with the biovolume, it is noted that while the maximum biovolume is related to an improvement in conditions for growth (nutrient in-put during column mixing periods) and reflected an increase in biomass, the maximum Chl_a is related to changes in cell pigment content and to spatial or successional trends in species dominance[32]. This importance is reflected in the fact that the Water Framework Directive (Directive 2000/60/EC) and official regulations of many countries specified that ecological status based on phytoplankton should be defined by measuring the biomass, composition and blooming events of the phytoplanktonic community[33]. All of which supports the use of biovolume as a metric in our research.

Remote sensing cyanobacteria biovolume can be done in two ways, indirectly through the determination of the phycocyanin concentration (PC), since it is their main pigment, or directly by determining their abundance or biovolume. The indirect method is the most common to estimate cyanobacterial biovolume using the MERIS hyperspectral sensor[34][35][33][18] and Landsat multispectral sensors[36]. However, before now no studies have been performed to estimate cyanobacterial biovolume directly with multispectral sensors using both subtropical and temperate reservoirs. Actually, according to a review by Johansen et al.[37], the top four empirical algorithm types for the detection and quantification HABs using remote sensing are the two-band difference algorithms (2BDA), the three-band difference algorithms (3BDA), the normalised difference (ND) and the fluorescence line height (FLH).

These algorithms, although published in previous studies and for other sensors, have been modified and adapted to be applicable to new optical sensors with different spectral and spatial resolutions[37]. The new satellites series of Copernicus European Union Earth's Observation Programme, called Sentinel, has been put into service the Sentinel-2 (S2-A and B) that carries the sensor MSI (Multispectral Instrument) whose measurement bands have interesting applications in the estimation of phytoplankton[38]. As for example for Chl_a spatial dynamics assessment[39], for phytoplankton spatiotemporal variation[40] and for a long-term spatial-temporal monitoring of eutrophication[41]. However, this multispectral sensor does not have a band centred in 620 nm, peak of phycocyanin absorption. Therefore, because while using S2 we do not have the theoretical band, we will try to improve the expertise for the cyanobacterial biovolume estimation by means of re-mote sensing directly.

In this paper we focus on the study of cyanobacterial biovolume, in order to calibrate and validate an algorithm for S2 images using an empirical approach. For this purpose, in situ samples of temperate and subtropical reservoirs and remote sensing reflectance of the MSI reflectance sensor were obtained. Furthermore, to observe its functionality and consistency, the algorithm will be applied on a biannual images series and calculate an average value for each image. In addition, these mean values will allow us to perform an annual comparative study between the temperate and subtropical zones. Direct estimation of cyanobacterial biovolume would allow continuous monitoring and could be used by water management authorities as a warning system to activate action plans.

Materials and Methods

Study site

The study site includes three river basins located in two different climatic zones. Two in the temperate zone, the Ebro river basin, located between 41° and 43° latitude with an area of 85,530 km^2, and the Xúquer river basin, located between 38° and 40° latitude an area of 42,989 km^2, both in Spain. And one in the subtropical zone, the Tietê river basin in Brazil, located between -20° and -23° latitude with an area of 72,391 km^2. A total of 24 field campaigns were carried out, 18 in the temperate zone and 6 in the subtropical zone. The locations of the basins and sampled reservoirs and lake are given in Fig. 1.

The 18 sampled reservoirs and one lake had total volumes ranging from 7×10^6 m^3 (Las Torcas) to $3{,}622 \times 10^6$ m^3 (Barra Bonita) and a maximum depth between 129 m in Contreras and 1 m in Albufera lake. Water quality is greatly influenced by the climate variability, and the reservoirs are classified in six climate types according to Köppen–Geiger classification: Cfa, Csa, Cfb, Csb, Bsh and Bsk in temperate zone and Cfa and Cfb in subtropical zone. Reservoir volume is rainfall, water temperature and human use de-pendent and varies greatly over the year, meaning that hydraulic residence time (HRT) oscillates from 0.03 yr (Riba-roja) to 2.15 yr (Alarcón). Furthermore, there are non-climatic factors, like altitude, which vary from 846 m.a.s.l. (meters above sea level) in Jacareí to 1 m.a.s.l. in Albufera. A summary of sampling sites specifications is specified in Appendix A.

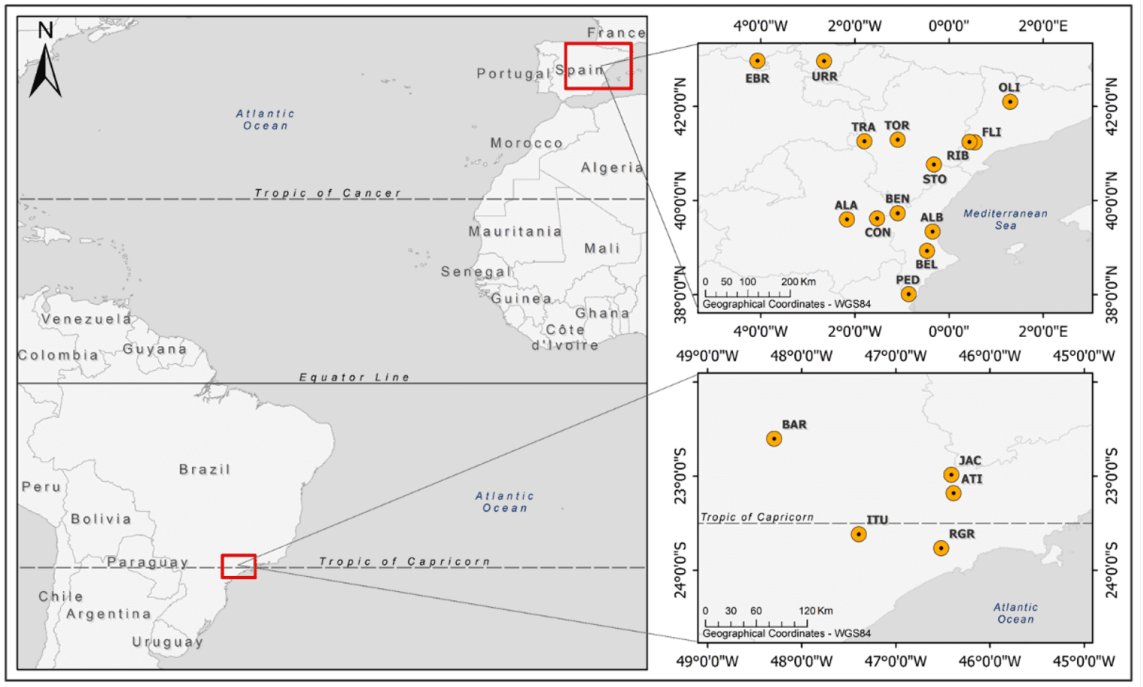

Figure 1. Locations of basins and reservoirs.

Field campaigns

From August 2016 to December 2021, a total of 24 field campaigns was completed and a total of 43 georeferenced samples were collected, 20 from the subtropical zone and 23 from the temperate zone. All samplings were complete except at 11 points in the sub-tropical zone, where no Chl_a or PC data were collected.

Samples were taken from a boat, using the GPS to reach one position situated more than one pixel of water away from the coastline and delimited by water pixels. When anchored, the point coordinates were geo-referenced with the GPS. Thereafter, the Secchi disc (white disk 20 cm Ø) was vertically immersed until it was no longer visible. The Secchi disc depth, a transparency measure, was used as the limiting depth for the integrated sample. To take the samples from the surface down to the sample depth a PVC tube or hydrographic bottle were used because integrated samples are more representative and avoid missing possible phytoplankton peaks[42].

The PC values were determined using fluorescence in vivo, both in situ and laboratory measurements. In the Xúquer and Tiête river basins PC was determined in situ using a C3 Submersible Fluorometer (Turner Design Instruments; San Jose, CA, USA). The fluorescence intensity at the pair Ex/Em = 590±30/≥645 nm was calibrated with a standard phycocyanin extract from *Spirulina* sp. (Sigma–Aldrich Chemicals). The main problems of fluorescence in vivo are the underestimation by large colonies[43] and effects of morphology[44], and the overestimation by light effects[45]. Nevertheless, Simis et al.[46] compared an in situ fluorometric approach and two extraction methods (freezing and thawing cycles and mechanical grinding) using some samples of water bodies located in our temperate zone, and

they concluded that the three methods for PC quantification showed similar values for concurrent measurements, but with high degree of scatter that suggested that PC ground truth measurements should be used with scrutiny. Indeed, the potential of PC fluorescence probes to monitor cyanobacterial biomass has been reported in several studies[47][48][49][43][50][14], and in addition, sample preservation and pigment extraction steps are not needed for in vivo florescence. However, regular calibration of the sensor is needed to get reliable data.

For Chl_a and PC laboratory analysis, the samples were preserved in darkness and refrigerated. Ebro river basin PC samples were analysed using the spectrofluorometer Hi-tachi FL-7000. The fluorescence intensity at the pair Ex/Em = 620/660 nm was referred to a standard phycocyanin extract from Spirulina sp. (Sigma–Aldrich Chemicals)[51]. For Chl_a analyses, firstly the water was filtered using 0.4–0.6-µm GF/F glass fiber filters, secondly the Chl_a was extracted using standard methods[52] and finally the concentration was calculated using Jeffrey and Humphrey[53] methods.

Phytoplankton samples were fixed in the field with Lugol solution, and were sedimented and counted under an inverted microscope Nikon-ECLIPSE TE-2000S in the laboratory according to the Utermöhl[54] method. Phytoplanktonic organisms were identified at the finest taxonomic possible level, and the biovolume was calculated by producing an approximate simple or compound geometrical shape for each specie[55][30][56]. The biovolume (μm^3 mL^{-1}) was estimated by multiplying the densities of each species by the average volume of each cell. The value obtained in μm^3 mL^{-1} was transformed into mm^3 L^{-1} by dividing this value by 10^6.

A linear correlation was established to observe the relationship of cyanobacterial biovolume with Chl_a and PC in the studied water bodies.

Image processing

The ESA S2 mission is based on a constellation of two identical satellites in the same orbit: S2A (launched in June 23, 2015) and S2B (launched in March 7, 2017). The MSI sensor is on board of each satellite, which measures the Earth reflected radiance in 13 spectral bands from VNIR (visible to near infrared) and SWIR (short-wave infrared), with a spatial resolution of 10, 20 and 60 m[57]. MSI bands number, spectral features and spatial resolution are shown in Table 1.

Band Number	Central wavelength (nm)	Bandwidth (nm)	Spatial resolution (m)
1	443.9	27	60
2	496.6	98	10
3	560.0	45	10
4	664.5	38	10
5	703.9	19	20
6	740.2	18	20
7	782.5	28	20
8	835.1	145	10
8a	864.8	33	20
9	945.0	26	60
10	1373.5	75	60
11	1613.7	143	20
12	2202.4	242	20

Table 1. MSI sensor band information[57].

The mission was initially optimised for studies on vegetation, urban planning and terrestrial ecosystems, but the inclusion of new bands in the red-edge (the limit of red and infrared spectral regions), its radiometric quality and its high spatial resolution has proven its usefulness for the study of inland waters[58].

Dataset of S2A and S2B imagery was downloaded from the ESA provider of Data and Information Access Services ONDA-DIAS. Software SentiNel Application Platform (SNAP; Brockmann Consult GmbH) was used for image processing. The images were resampled at 10 m with SNAP interpolation tools, because bands used have different spatial resolution. Thereafter a subset was made of the water body, which was atmospherically corrected by the Case2 eXtreme (C2X) neuronal net. This choice was based on two factors: the model training range and the previous studies results on its assessment. Regarding the training range, C2X is the net with the widest range of inherent optical properties[59]. As for its assessment, we focus on the high wavelength bands because the study area has very eutrophic waters, and waters with high Chl_a (above 3-5 mg m^{-3};[60]) produce distinguishable spectral characteristics in the red and NIR regions of the reflectance spectrum[61]. In addition, previous studies such as

Pereira-Sandoval et al.[62], Pahlevan et al.[63], Tavares et al.[64] and Sòria-Perpinyà et al.[65] have demonstrated that C2X improves its results for longer wavelength bands, better reproducing the in-creased scattering in the NIR and demonstrating their best results for turbid waters. The remote sensing reflectance (Rrs) values were extracted by applying a window of 3x3 pixels centred in field coordinates, to avoid possible anomalies in the values.

A total of 24 images close to the 24 data campaigns (43 samples) were used for retrieval the algorithm. Regarding the time-window between image acquisition and sampling, 19 samples matched the image, 6 with one-day difference, 9 with two days difference, 7 with three days difference, and only 2 samples had four days difference. The time-window between image acquisition and field campaigns was extended to four days, considering two factors: (1) HRT (Table A1)—calculated as the ratio between the reservoir's average daily outlet and the reservoir's total volume; and (2) meteorological changes—we checked the values of temperature, wind, and rain between the image and sample data in most lakes. Meteorological stability was checked for the temperate zone at the open data web page of the Spanish State Meteorological Agency (https://opendata.aemet.es/centrodedescargas/productosAEMET), and for the subtropical zone at the meteorological data bank of Brazil National Meteorological Institute (https://portal.inmet.gov.br/dadoshistoricos). Finally, regarding our 24 samples that did not coincide with the images, we did not observe days with rain, the wind did not exceed 10 km/h and temperature was stable in its daily oscillations.

Retrieval algorithm

The retrieval algorithm was obtained empirically by generating a regression model for operations with bands for temperate and subtropical zones data. The empirical approach generally produces robust results for the areas and data sets from which they are derived, and have a demonstrable capability to provide timely and accurate information for a variety of parameters in lakes and estuaries that can be used for diverse applications[66].

In the following paragraphs, we will present the different algorithms tested in this work by grouping them into six empirical algorithm types: simple band, 2BDA, multiple linear regression (MLR), 3BDA, ND and FLH (Table 2). Only one simple band was tested, the 665 nm band, which was used in the study of Viso-Vázquez et al.[67] obtaining good results using S2 to determine PC in a eutrophic reservoir.

Regarding the simple ratio 2BDA, the ratio for pigments determination is expressed between the wavelength located at maximal scattering by algal cells (minimal absorption by pigments) and the wavelength location at maximal pigment absorption efficiency[68][69]. PC absorption is centred at 620 nm and Chl_a absorption is centred at 665 nm, while the maximal scattering by algal cells is situated at about 700 nm. Following this bio-optical base we test the ratio with maximum algal dispersion (B4=704 nm) and the majority pigment (B3=665 nm) because the MSI sensor does not have a 620 nm band. This ratio reached good results using S2-MSI images of temperate region reservoirs in the study of Sòria-Perpinyà et al.[29] to determine Chl_a and PC and in the study of Pérez-González et al.[51] to determine PC. Another 2BDA is the ratio $R740/R665$, used by Sòria-Perpinyà et al.[58] and reaching good results to

determine PC in a hypertrophic lagoon. It is also possible to use a MLR with the ratios *R*565/*R*482 and *R*660/*R*482, as applied by Isenstein et al.[36] to a multispectral sensor, the Enhanced Thematic Mapper Plus on board Landsat 7, to obtain cyanobacterial biovolume indirectly through PC. These ratios become as follows with the MSI sensor bands: *R*560/*R*490 and *R*665/*R*490.

The 3BDA tested was developed by Gitelson et al.[69] for vegetation, and applied in turbid productive water by Dall'Olmo et al.[70] using in situ reflectance of three spectrum points: 660–670 nm, 720–730 nm and 740–750 nm. These spectrum points were adapted to S2-MSI using B4 (665 nm), B5 (704 nm)-out of range- and B6 (740 nm). This model was applied in previous studies by Sòria-Perpinyà et al.[71] to determine Chl_a in a hypertrophic lagoon and by Cairo et al.[72] to determine Chl_a in a tropical reservoir.

In relation to the normalised difference (ND), we tested three algorithms. The first is based on the study of Medina-Cobo et al.[33] using the MERIS hyperspectral sensor to determine cyanobacterial biovolume indirectly through PC, obtaining good results with a ND between 704 nm and 620 nm bands in temperate reservoirs. However, because the MSI sensor does not have 620 nm band, we used the 665 nm band, resulting the normalised difference chlorophyll index (NDCI) of Mishra and Mishra[73] for MERIS, which was applied to S2-MSI by Caballero et al.[74] to obtain HAB's detection in complex coastal waters. The second ND used 865 nm and 665 nm wavelengths, applied by Khalili and Hasanlou[75] in a tropical zone using S2 to determine HAB presence. The third ND was obtained by Cillero-Castro et al.[76], using 560 nm and 490 nm bands to determine Chl_a with S2 in a reservoir located in the Atlantic Biogeographical Region, obtaining good results when applied to locations that typically have lower Chl_a (<5 mg m^{-3}).

The last empirical algorithm type tested was the FLH developed by Wynne et al[77] to determine the HAB presence. The algorithm is the Cyanobacteria Index (CI), a "spectral shape" (or curvature) algorithm, which is a form of the second derivative around the 681 nm[77]. However, the band nearest to 680 nm for S2-MSI sensor is B5 (704 nm), and the peak at 700–710 nm, just to the right of 681 nm, is caused when phytoplankton and scatterers are present in large concentrations and the strong scattering greatly exceeds fluorescence[78].

Algorithm type	Equation	S2 Bands	Estimation	Reference
Band	$Rrs665$	$B4$	PC	[67]
2BDA	$\frac{Rrs704}{Rrs665}$	$\frac{B5}{B4}$	Chl_a	[29]
			PC	[29]
				[51]
2BDA	$\frac{Rrs740}{Rrs665}$	$\frac{B6}{B4}$	PC	[58]
RLM	$\frac{Rrs560}{Rrs490}; \frac{Rrs665}{Rrs490}$	$\frac{B3}{B2}; \frac{B4}{B2}$	PC	[36]
3BDA	$\left(\frac{1}{R665} - \frac{1}{R709}\right) \times R740$	$\left(\frac{1}{B4} - \frac{1}{B5}\right) \times B6$	Chl_a	[69]
ND	$\frac{Rrs704 - Rrs665}{Rrs704 + Rrs665}$	$\frac{B5 - B4}{B5 + B4}$	PC	[73]
ND	$\frac{Rrs865 - Rrs665}{Rrs865 + Rrs665}$	$\frac{B8A - B4}{B8A + B4}$	HAB presence	[75]
ND	$\frac{Rrs560 - Rrs490}{Rrs560 + Rrs490}$	$\frac{B3 - B2}{B3 + B2}$	Chl_a	[76]
FLH	$Rrs704 - Rrs665 + (Rrs665 - Rrs740) \times \frac{704 - 665}{740 - 665}$	$B5 - B4 + (B4 - B6) \times \frac{704 - 665}{740 - 665}$	HAB presence	[77]

Table 2. Tested algorithms summary.

Accuracy assessment

The process to obtain the best algorithm was carried out using the Spectral Index (SI) assessment toolbox[79] in the Automated Radiative Transfer Models Operator (ARTMO) package[80]. Using the SI, the tested algorithms where defined and evaluated with k-fold cross validation. The advantage of using a k-fold cross-validation sampling is that all data are used for both training and validation, and each single observation is used for validation exactly once, returning a more robust estimate of the model's performance, by aver-aging statistics from multiple independent training and test subsets[81]. To generate our results, a 4-fold cross-validation sub-sampling procedure was applied, and the multiple goodness-of-fit measures like the R^2, the root mean squared error (RMSE) and the normalized

RMSE (NRMSE (%) = RMSE / (value range of parameters as measured in the field) × 100) were then averaged over the 4 subsets.

In summary, with the SI toolbox, the tested algorithms and the cyanobacterial biovolume data (raw or transformed - Log_{10} and square root-), were correlated using various curve fitting functions (linear, potential, exponential or polynomial).

WHO surveillance levels

In accordance with the WHO (World Health Organization), the limits established by Chorus and Welker[15] were applied to the cyanobacterial biovolume estimated values. The surveillance limits for drinking and bathing waters for the health monitoring of cyanobacteria are given in Table 3.

Drinking waters	**Bathing waters**	**Density (cell ml^{-1})**	**Biovolume (mm^3 L^{-1})**	**Chlorophyll *a* (mg m^{-3})**
Vigilance level	Vigilance level	200	<0.3* / 1-4**	<1* / 3-12**
Alert level I	Guidance level 1	2,000	≥0.3* / 4-8**	≥1.0* / 12/24**
Alert level II	Guidance level 2	100,000	≥4* / >8**	≥12* / >24**

Table 3. Surveillance limits according to WHO. Density, biovolume and chlorophyll a limits are extracted from Chorus and Welker[15].

Guidance level 1: Low probability of adverse health effects.

Guidance level 2: Moderate probability of adverse health effects

**Drinking waters; **Bathing waters*

Annual variation

For the annual temporal variation, images covering several reservoirs, one from the Ebro river basin and one from the Tietê river basin, were used. The best images (cloud-free or partly cloud-free) of 2021 and 2022 were processed for each area. A total of 38 images were downloaded, 18 of the temperate zone and 20 of the subtropical zone. After resampling and before the atmospheric correction, an image subset was selected (Fig. 2).

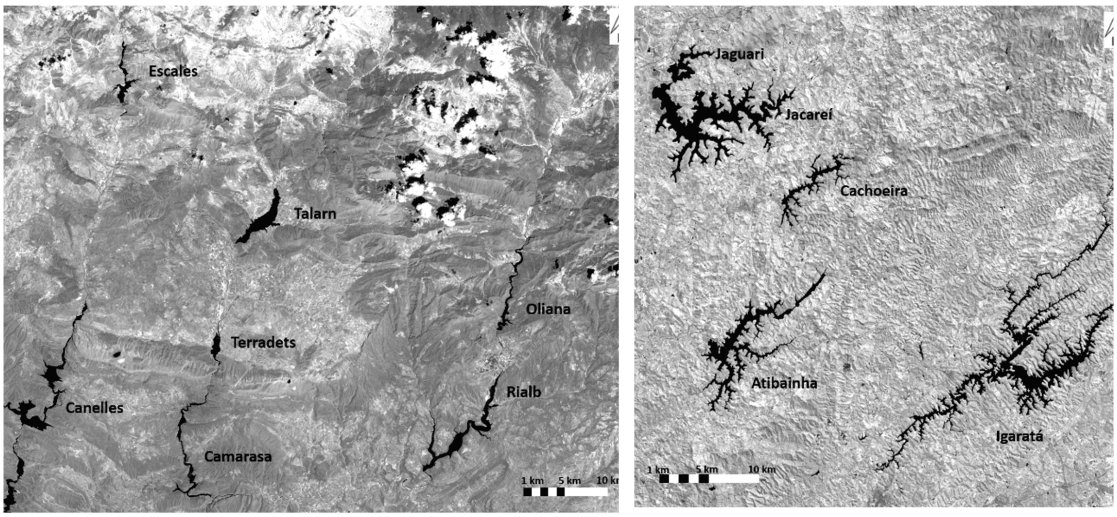

Figure 2. Images subsets used for the cyanobacterial biovolume annual temporal variation study: (**a**) Ebro river basin (Spain); (**b**) Tietê river basin (Brazil).

The obtained algorithm was applied in the reservoirs that appear completely in the image using a region of interest, also avoiding cloudy affected areas. Finally, the thematic maps were presented using the band 8a as background.

For the cyanobacterial biovolume annual temporal variation graphical representation, the mean and maximum error for all water bodies of each processed image was calculated using the statistics tool of the SNAP programme. The clouds modify the available pixels of each reservoir in each image, and each reservoir has a different ecological status. To avoid an influence in the mean and maximum error values due to the available pixels of each reservoir, firstly was calculated a mean and maximum error for each reservoir and with these values the global image mean and maximum error was calculated to plot.

Results

Field data

A total of 43 samples were collected on 19 different water bodies between 2016 and 2021 in different projects. The cyanobacterial biovolume values were highly variable, ranging with a minimum of 0.001 mm^3 L^{-1} registered in Benaixeve reservoir in June 2020 and the maximum of 297.7 mm^3 L^{-1} registered in Itupararanga reservoir in October 2017 by dos Santos Machado et al.[82]. The dataset has an average of 37 mm^3 L^{-1} and a standard deviation of 63.6 mm^3 L^{-1}.

The variability of these samples reach several WHO guide levels for drinking waters: 22 are classified in the vigilance level, 6 in the Alert level I and 15 in the Alert level II. Regarding water bodies, 4 reservoirs were in the vigilance level in all samples, 10 reservoirs were classified in Alert level I, the level with more water bodies classified, and 4 water bodies were classified in the Alert level II; three reservoirs (Bellús, Barra Bonita and Itupararanga) and Albufera lake. Only La Tranquera, had one sample in the vigilance level and two samples in Alert level I.

The relationship of cyanobacterial biovolume with Chl_a (Fig. 3a) and PC (Fig. 3b) shows a direct and significant correlation for both variables, with coefficients of de-termination of 0.66 and 0.73 respectively. As expected, the correlation is higher with PC since it is their main pigment. The representation of the cyanobacterial biovolume values on a logarithmic scale allows us to observe that beyond a threshold the relationship is no longer direct. In both cases this is observed in the fit equation intercept value, which corresponds to a Chl_a of 5.5 mg m^{-3}, and a PC of 11.6 mg m^{-3}.

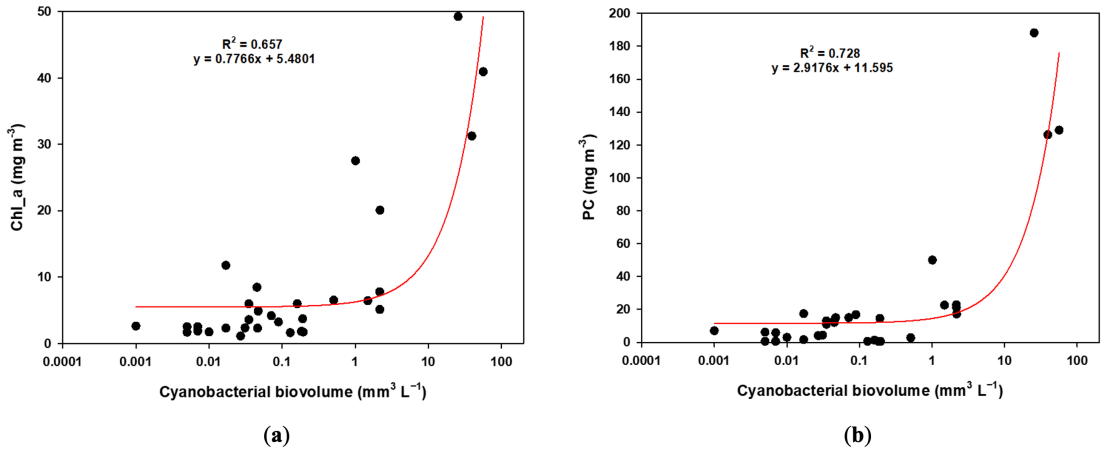

Figure 3. Linear correlation between cyanobacterial biovolume in log scale and Chl_a (**a**) and PC (**b**).

Retrieval algorithm

In the 4-fold cross-validation process, we tested nine algorithms: one band, one MLR, two ratios, three ND, one 3BDA and one FLH (Table 2). The results averaging the R^2 from the 4 independent training and test subsets were statistically significant ($p < 0.001$) for five algorithms (Table 4), while for four algorithms the results were non-significant (R665, MLR, NDB3B2 and FLH). The correlation between cyanobacterial biovolume and band combinations showed a positive direction for cyanobacterial biovolume, with higher values indicating higher concentration except for the FLH.

Regarding the other goodness-of-fit measures the RMSE and NRMSE were calculated (Table 4). The best result was a polynomial regression obtained with the NDB5B4 and transformed cyanobacterial biovolume with square root, with

doi.org/10.32388/IEUZZR

a RMSE of 1.71 mm^3 L^{-1} and a NRMSE of 7.6%.

	*Rrs*704/*Rrs*665	*Rrs*740/*Rrs*665	NDB5B4	NDB8AB4	3BDA
(data, function)	(√,polynomial)	(√, linear)	(√, polynomial)	(√, linear)	(√, linear)
R^2	0.90	0.79	0.92	0.72	0.91
p	<0.001	<0.001	<0.001	<0.001	<0.001
RMSE	1.93	4.18	1.71	5.81	1.84
NRMSE	8.1	11.9	7.6	14.0	7.9

Table 4. K-fold cross validation statistically significant results.

data=used data (transformed values with Log10 or square root).

The correlation between in situ and estimated values by NDB5B4 algorithm is shown in Fig. 4. However, the fit line suggests that the algorithm tends to underestimate biovolume values under 0.01 mm^3 L^{-1}.

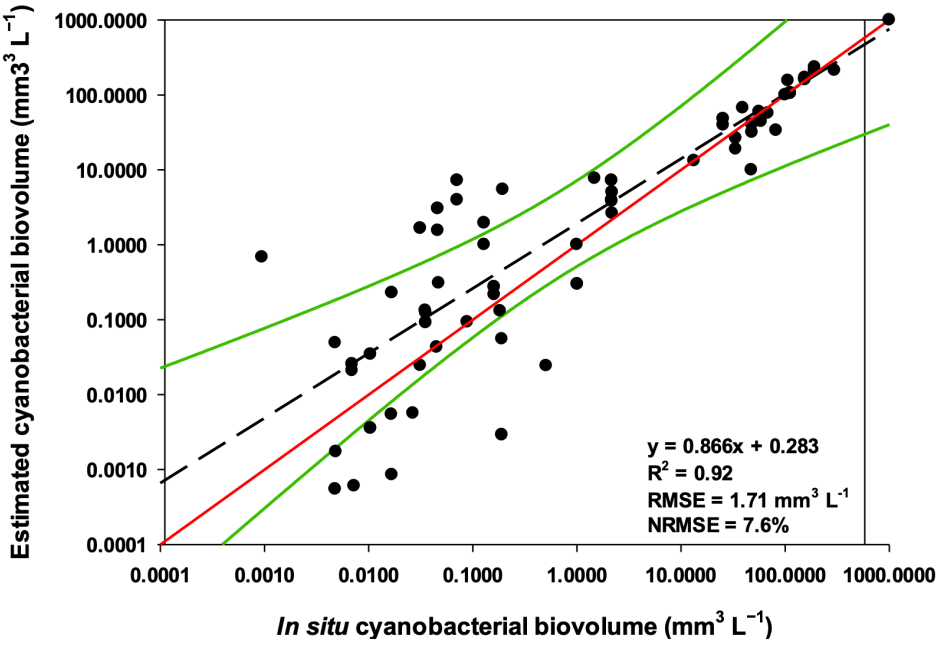

Figure 4. Algorithm validation, observed versus predicted data in log scale. Red line is 1:1, dashed line is the adjustment and the green lines are the 99% interval confidence.

doi.org/10.32388/IEUZZR

Finally, the best performing algorithm using the entire database is shown in Fig. 5. The representation of the cyanobacterial biovolume square root values on a logarithmic scale allows us to observe that beyond a threshold the relationship is no longer direct. This threshold is situated at 0.1, corresponding to 0.01 mm^3 L^{-1}. If we apply this value to the equations obtained from Chl_a and cyanobacterial biovolume correlation and PC and cyanobacterial biovolume correlation, the values obtained are 5.4 and 12.4 mg m^{-3} respectively, which are values similar to the fit equation intercept values.

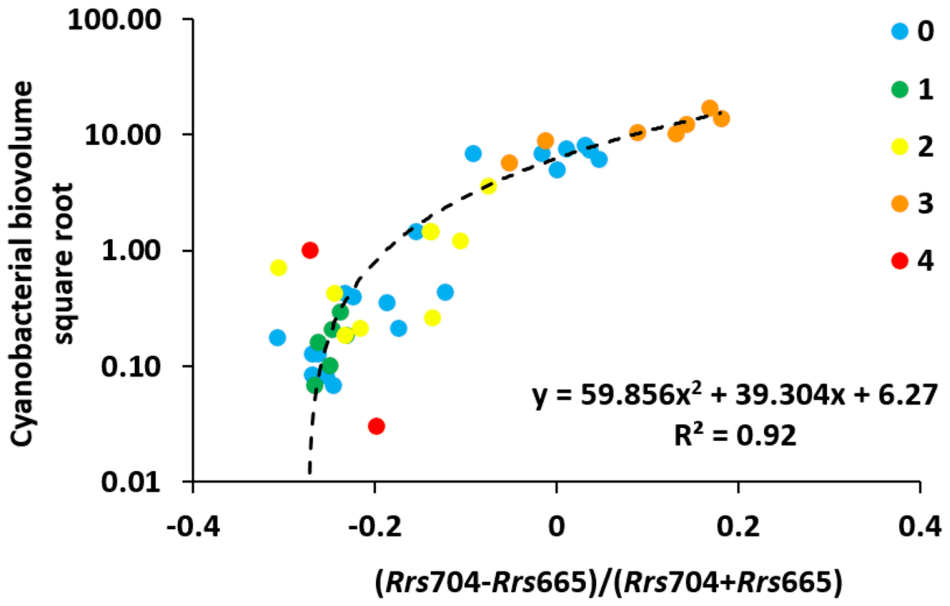

Figure 5. Cyanobacterial biovolume square root algorithm in log scale. The colour-coded represent the time difference in days between in situ samples and image day.

Image output

Once the algorithm was obtained, to observe its functionality and consistency, equation 1 was applied to S2-MSI images.

$$Cyanobacterial\ biovolume = \left(59.856 \times \left(\frac{Rrs704 - B665}{Rrs704 + B665}\right)^2 + 39.304 \times \left(\frac{Rrs704 - B665}{Rrs704 + B665}\right) + 6.27\right)^2 \quad (1)$$

The aim is to compare three aspects; a first comparison would focus on the climate zones differences (range of values), a second comparison would focus on differences within annual temporal variation (moments of the minimum and maximum cyanobacterial biovolume), and a third and final comparison would focus on spatial variation (tail-dam asymmetry).

doi.org/10.32388/IEUZZR

The two first comparisons are shown in the annual temporal variation of the cyanobacterial biovolume mean values for two areas, one from temperate and one from subtropical zones (Fig. 6). Regarding the range of values, it can be observed that the highest values were recorded in the subtropical zone. While the temporal variation of the studied years was different between the two climatic zones with more variations in the subtropical zone, although the highest values were estimated for 2022 in both climatic zones. The period when the minimum values were recorded in the temperate zone was in late spring (June), coinciding with a relative minimum value in the subtropical zone during the dry period. On the other hand, the maximum values in the temperate zone were observed in autumn (October), which is a period of increase in cyanobacterial biovolume in the subtropical zone (November), coinciding with the beginning of the humid period. However, in the subtropical zone several relative minimum and maximum values were observed, and the coincidences between the two years studied were the minimum value registered at the middle of the dry period (June) and the maximum values registered at the beginning of the humid period (November), while other relative maximums and minimums not heaved coincidences. Regarding the WHO surveillance levels, the mean values of the Ebro basin were under bathing waters guidance level 2 during the first half of 2021 and in the late spring of 2022, while the mean values of the Tietê basin were always above this level. Furthermore, the mean values of the Tietê basin overcome the bathing guidance level 2 during the entire period, with moderate probability of adverse health effects, therefore toxin analysis should be performed.

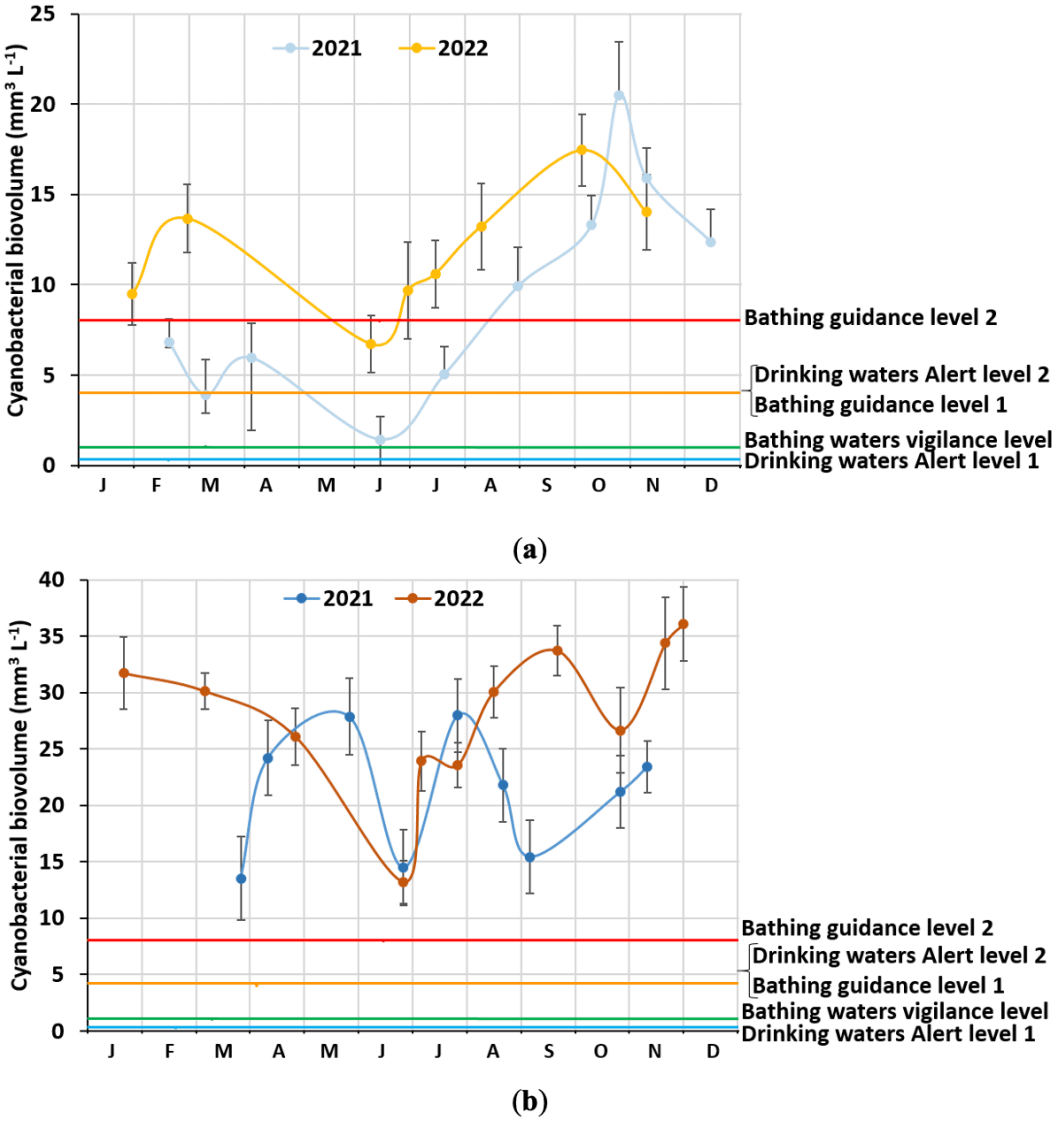

Figure 6. Annual variation of the median cyanobacterial biovolume estimated values for each processed image from temperate zone (a) and subtropical zone (b).

A maximum value was observed during spring in the temperate zone, and an increase in the biovolume of cyanobacteria since the annual minimum (June) until the end of autumn was observed (October-November). The peaks and troughs of the annual variation of cyanobacterial biovolume in the subtropical zone do not coincide completely over the years studied. Since the reservoirs function is to retain water in rainy periods for use at other moments, the reservoirs hydrodynamics may be determining the plankton temporal variation. For this reason, we present the annual water volume variation for each reservoir (Fig. 7) that appear in the images of the temperate and subtropical zones (Fig. 2). A relationship can be seen between the minimum reservoir volumes values and the

doi.org/10.32388/IEUZZR

maximum mean value of the cyanobacterial biovolume estimated values, both in October-November, although there are other relative maxima in the subtropical zone.

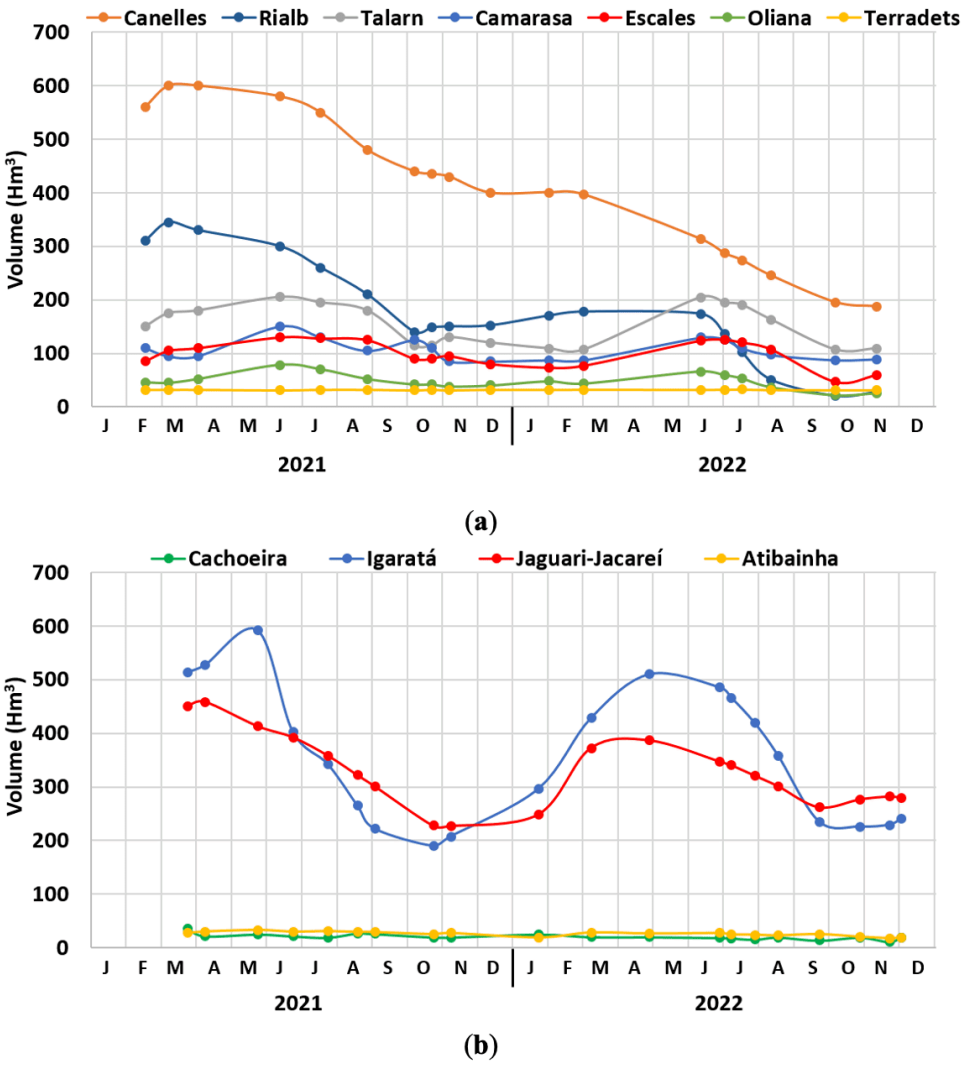

Figure 7. Reservoir volumes annual variation for each reservoir of the temperate zone (a) and subtropical zone (b) images.

The linear correlation between the mean cyanobacterial biovolume and the reservoir volume for the same day of image was also obtained for each reservoir (Table 5). For the temperate zone, the results indicated a negative correlation in the 7 reservoirs, but statistically significant in 6. Whereas in the subtropical zone, the results indicated also a negative correlation in all reservoirs, but only 2 were statistically significant.

doi.org/10.32388/IEUZZR

Reservoirs	r	p value
Canelles	-0.596	0.01
Rialb	-0.760	0.001
Talarn	-0.743	0.001
Camarasa	-0.507	0.05
Escales	-0.610	0.01
Oliana	-0.752	0.001
Terradets	-0.202	n.s.
Iagartá	-0.278	n.s.
Jaguari-Jacareí	-0.363	n.s.
Atibainha	-0.528	0.05
Cachoeira	-0.510	0.05

Table 5. Pearson correlation and significance value for the correlations between the median cyanobacterial biovolume estimated values and reservoirs volumes.

n.s.= non-significant ($p > 0.05$).

To observe the spatial variation within the reservoirs, four images corresponding to the 2021 annual variation of the cyanobacterial biovolume for both climatic zones are shown in Figure 8. The images from the temperate zone (Spain) correspond to late spring as the minimum value and to autumn as the maximum value (Fig. 8a). The images from the subtropical zone (Brazil) correspond to March as the minimum value, at the end of the rainy season, and to May as the maximum value, during the dry season (Fig. 8b). Regarding the spatial variation, it is mostly observed in the reservoirs with the highest values of cyanobacterial biovolume, with a reduction in cyanobacterial biovolume in the tail-dam direction. All images processed for the annual series are shown in Appendix B.

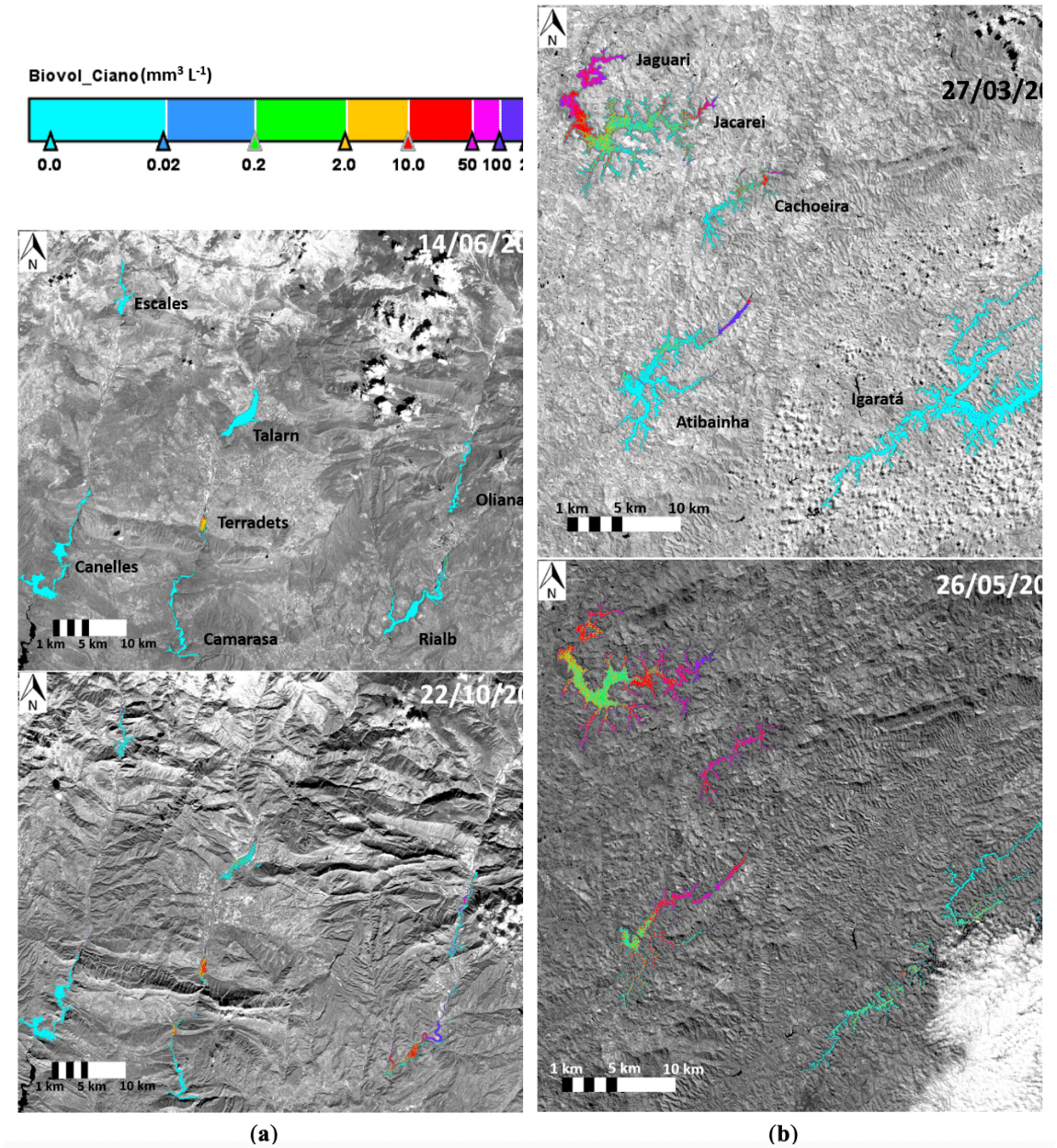

Figure 8. Cyanobacterial biovolume of some reservoirs: (**a**) Ebro basin reservoirs (Temperate zone). Image of 14 June (up) and 22 October (down) 2021; (**b**) Tietê basin reservoirs (Subtropical zone). Image of 27 March (up) and 26 May (down) 2021.

Discussion

Field data

Direct cyanobacterial-related variable quantification, in cell density, biovolume or PC using remote sensing is complicated without the band at 620 nm, in the phycocyanin maximum absorption. This difficulty increases when

doi.org/10.32388/IEUZZR

working with such a heterogeneous cyanobacterial biovolume data range, 0.001—297.7 $mm^3\ L^{-1}$. This data range has a direct linear relationship with both Chl_a and PC values, although this relationship is not effective until it exceeds the threshold of 5.5 mg m^{-3} for Chl_a and 11.6 mg m^{-3} for PC. This PC threshold is also observed in the study by Medina-Cobo et al. [33] for temperate region reservoirs, obtaining a coefficient of determination of 0.6.

Retrieval algorithm

This heterogeneity makes it particularly difficult to obtain acceptable errors to consider the applicability of the algorithm. The better coefficients of determination between the field and estimated data reaches a R^2 of 0.92, obtained with the NDB5B4. Reaching a good coefficient of determination such as Medina-Cobo et al.[33] using MERIS (R^2 = 0.72), even though they have no error to compare. The other work using cyanobacterial biovol-ume was performed by Isenstein et al.[36] with a multispectral sensor, but their biovol-ume range is much lower, only until 0.21 $mm^3\ L^{-1}$, so a comparison would be unrealistic.

The retrieval algorithm results, which were obtained using subtropical and temperate water bodies samples, make evident the breadth of the retrieval algorithm to estimate cyanobacterial biovolume from S2 images. The use of the NDB5B4 to retrieve phytoplankton variables coincides with bands used in other studies to estimate different variables expressing the presence of phytoplankton. The S2 bands are few and widely spaced, so by using an empirical model it is possible to use B5, with maximum algal dispersion (705 nm), and B4, with the majority pigment absorption (665 nm), combinations to estimate Chl_a[83][84][85][29], PC[58][51] or phytoplankton biovolume (this study). Furthermore, in our case, taking the band difference and normalizing by the sum of their reflectance, eliminate any uncertainties in the estimation of Rrs, seasonal solar azimuth differences, and atmospheric contributions at those wavelengths[73]. Aspects that improve the results of NDB5B4 respect to the others tested algorithms.

This result is expected because empirical methods are limited in their ability to dis-criminate between non-unique signals from parameters that may be covariant, for example, total suspended solids and Chl_a[66]. For this reason, the likely sensitivity of red-peak/scattering approaches is limited to concentrations greater than approximately 10 mg m^{-3} for which biomass the red peak from scattering becomes apparent[86]. For our algorithm, the correlation between Chl_a and cyanobacterial biovolume establishes our detection limit at 5 mg m^{-3} of Chl_a.

The thresholds established by the correlations between Chl_a and PC values and cyanobacterial biovolume values do not coincide with those established by the WHO. This is because, as Kelly et al.[87] demonstrate in their study, this relationship varies with nutrient concentrations, growth stage and species composition, which impact pigment concentrations and absorption spectra. This in turn means determining accurate relationships between absorption spectra and biovolumes is challenging. However, we consider our algorithm as a good tool for monitoring the guidance levels of WHO in our study area because it limit is 0.01 $mm^3\ L^{-1}$. And although the algorithm

underestimates biovolumes values under this threshold, these values are above the WHO vigilance level for drinking and bathing waters. Other question is overestimate biovolume values upper this threshold but, in this case, it is preferable to obtain values above the surveillance level and alert level 1 and activate the warning system, rather than the opposite. Nevertheless, for more accurate monitoring, sometimes a control sample will have to be carried out to verify the predicted values with field observations and to recalibrate the algorithm.

Image output

Regarding the images processed to observe the algorithm applicability and its coherence (Appendix B), the algorithm behaves correctly. But when looking the images of Appendix B, note that not all reservoirs follow the same annual variation explained in Fig. 6, were is represented the global image mean, obtained with the means of all reservoirs than appear in the image subset (Fig. 2). As obtained in the field campaigns, much higher values were estimated in the subtropical zone than those estimated for the temperate zone.

The variations of biovolume thorough the year is related with the water column mixing. In the dimictic reservoirs of the temperate zone there are two periods of mixing, periods coinciding with the two cyanobacterial biovolume maximums in spring and autumn. Nevertheless, the highest values were recorded in autumn. This is due to the hydrological reservoirs managements, with a management that greatly deplete the reservoirs volumes during the summer for agricultural uses, play an important role. Outflow causes a sharp drop in the reservoir levels, and variations in the volumes and heights of the reservoirs can generate excess of particulate matter because of coastline instability, which facilitates the dragging of particulate matter due to the effect of waves[88]. Sediment removal releases nutrients and leachates, triggering phytoplankton proliferation[89], which is concentrated by the water volume reduction. Conditions where cyanobacteria will proliferate better due to adaptations such as low light requirements[8][9] and buoyancy regulation mechanisms[12].

In the tropical zone, with high cyanobacterial biovolume values during the entire studied period, specially in 2022, the minimum values were registered at the middle of the dry period (June), and the maximum values were registered at the beginning of the humid period (November). Similar pattern to that describer by Oliver and Ribeiro[90] in a study of monthly cyanobacteria density for the period 2010–2012 for a reservoir in the Metropolitan Region of São Paulo, were observe an increasing proliferation at the start of the rainy season in the early spring (October), maintained at a high level until the decrease of rain-fall and temperature in April. But other authors observe that biovolume increases shortly after the rainy season with a maximum recorded during the dry period[91]. In this sense, 2021 cyanobacterial biovolume variation coincides with the study by Tundisi et al.[92] in a Tietê Basin reservoir, where they record a maximum production during winter period (May-June-July) and lower production during the summer (December to March), but due to clouds, we do not have images for the rainy season in 2021. Regarding the relative minimum and maximum values, our 2021 annual variation shows a similar pattern to that of the Oliver and Ribeiro[90] with three annual relative maximum and minimum values. The difference between the

two studies is the month when they occur. In Oliver and Ribeiro[90] the maximum values were registered in March, June and November and in our study the maximum values were registered in May, July and November, while the minimum values were registered in February, May and September in the Oliver and Ribeiro[90] study but in this study, they were registered in March, June and September. Note that they use a monthly average, while we only have a point value, and phytoplankton have a high replication rate (e. g. [93]). These variations of biovolume thorough the year is related also with the water column stratification of polymictic reservoirs. Hydrology of the basin, retention time of the reservoir and climatic events have an impact in the vertical and horizontal structure of the system promoting rapid changes in the plank-tonic community[92].

However, although the results may seem realistic, it would be necessary to do yearly monitoring with in situ data to improve the level of accuracy in order to avoid the overestimation of low cyanobacteria levels, since our algorithm is based on point data which does not represent a hydrological year.

Regarding the spatial variation, in addition to reducing the concentration of nutrients and suspended solids, the reservoirs regulate and reduce the variability of the flows of these variables[94]. This occurs also with the cyanobacterial biovolume spatial variation, with a tail-dam asymmetry observed in many reservoirs of the processed images, both in the temperate and subtropical zones.

Considerations

The methodology applied to S2 images increases our real-time information of cyanobacterial biovolume and spatial heterogeneity in lakes and reservoirs with concentrations subject to monitoring according to WHO protocol, which are impossible to highlight using current field sampling techniques. This method allows us to control the WHO monitoring values before carrying out more exhaustive in situ sampling, and therefore serves as a warning method. Furthermore, since S2 mission will provide images over the next decades, due to S2 being one of the key missions of the Copernicus program, the methodology will be applicable to a wide variety of water bodies over the tropical and temperate zones. To apply the established algorithm, the main points of uncertainty would be the field data, the reflectance data and estimation data. Regarding the field data, a regular calibration of the sensor is needed to get reliable data. Respect to the reflectance data, low uncertainty surface reflectance products are essential. For this work, the algorithm has been developed from reflectance obtained with a given acceptable uncertainty atmospheric correction, however it could be readjusted to a future less uncertainty atmospheric correction using the same ND and with new field data. Finally, regarding the estimation data, use the ND reduce the uncertainties in the estimation by excluding the seasonal solar azimuth differences and atmospheric contributions[39].

Monitoring of cyanobacterial blooms is becoming increasingly important, and the results obtained here show the capabilities of S2 in this regard. Therefore, we can deduce that it would be good to incorporate remote sensing as a tool in routine monitoring plans to be taken in areas with high and medium risk of cyanobacterial blooms, such as those presented by Funari et al.[95] and Chorus and Welker[15] in their works. And can be used as a method to

facilitate the study of HAB's frequency as a climate change consequence effect. There are works in this area, such as the research carried out by Oyama et al.[96] to monitor levels of cyanobacterial blooms using a multispectral sensor, and the work of Jia et al.[97] using a hyperspectral sensor to determine cyanobacterial bloom frequency, although without cyanobacterial quantification.

The results obtained provide an algorithm for the cyanobacterial biovolume space-temporal monitoring. It is relevant because it is the first time that a cyanobacterial biovolume direct retrieval algorithm is obtained with real S2 data using samples from temperate and subtropical zones. Cyanobacterial biovolume quantification will not only allow us to establish the WHO surveillance levels for drinking and bathing waters, but also to know the amount of biomass generated by the cyanobacteria, maybe toxic, which will subsequently degrade by consuming oxygen and/or be incorporated into the sediment. Furthermore, the results contribute to the knowledge of the phytoplankton pigments and cyanobacterial biovolume relationship.

Conclusions

The cyanobacterial biovolume can be estimated directly from S2 images using NDB5B4. Such as S2 bands are few and wide, the same bands can be used to estimate different variables that express phytoplankton presence, like Chl_a, PC and cyanobacterial biovolume.

The application of the algorithm developed in images has demonstrated its functionality and consistency, reproducing both the cyanobacterial biovolume annual variation and the spatial variation patterns characteristic of reservoirs. The highest values were al-ways recorded in the subtropical zone. The temporal annual variation in the temperate zone registered a minimum annual value in the late spring and a maximum annual value in the late autumn. More variations were registered in the subtropical zone, with diverse relative maximums and minimums thorough the year. A tail-dam asymmetry was observed in the processed images, both in the temperate and subtropical zones.

The algorithm developed for S2 images increases our real-time presence, the cyano-bacterial biovolume information and spatial distribution in lakes and reservoirs of potentially toxic cyanobacteria. In addition, it can be employed as an early warning system by comparing it with the threshold limits set by WHO and to quantify the quantity of biomass generated by cyanobacteria, which may be toxic, and which will have to be absorbed by the ecosystem.

Appendix A

Name	Abbreviation	Depth	Volume	Elevation	HRT	Climate	Visits	Samples
		m (max.)	x10^6 m^3	m.a.s.l.	years			
Alarcón	ALA	71	1118	806	2.15	Csa	2	2
Albufera	ALB	1	360	1	0.1	Csa	1	1
*Atibainha	ATI	25	303	790	0.29	Cfb	1	4
*Barra Bonita	BAR	25	3622	430	0.20	Cfa	1	1
Bellús	BEL	34	69	144	0.24	Csa	1	2
Benaixeve	BEN	90	221	450	0.63	Csb	1	1
Contreras	CON	129	852	669	1.48	Csa	1	3
Ebro	EBR	24	540	838	1.27	Cfb	1	1
Flix	FLI	26	11	41	0.00	Bsk	1	1
*Itupararanga	ITU	21	286	843	0.67	Cfb	2	11
*Jacareí	JAC	33	1083	846	1.01	Cfb	1	3
La Tranquera	TRA	43	84	685	0.71	Cfa	3	3
Las Torcas	TOR	41	7	624	0.27	Cfb	1	1
Oliana	OLI	73	101	518	0.08	Cfa	2	2
Pedrera	PED	60	246	50	-	Bsh	1	3
Riba-roja	RIB	34	210	70	0.03	Bsk	1	1
*Rio Grande	RGR	42	116	745	-	Cfb	1	1
Santolea	STO	44	48	583	0.60	Cfa	1	1
Urrunaga	URR	24	72	547	0.37	Cfb	1	1
Total							24	43

Table A1. Summary of sampled lake and reservoirs. Symbols and abbreviations: max.: maximum; m.a.s.l.: meters above sea level; HRT: hydraulic residence time; *Subtropical zone.

doi.org/10.32388/IEUZZR

Appendix B

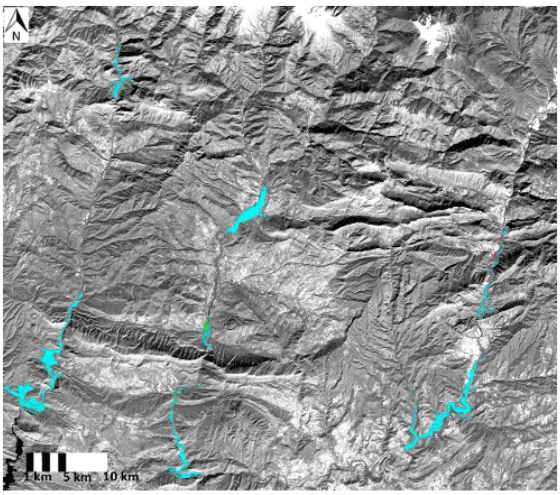

(a) 19/02/2021

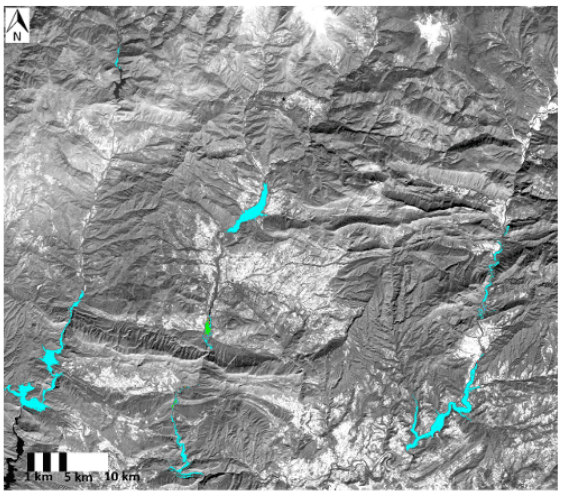

(b) 11/03/2021

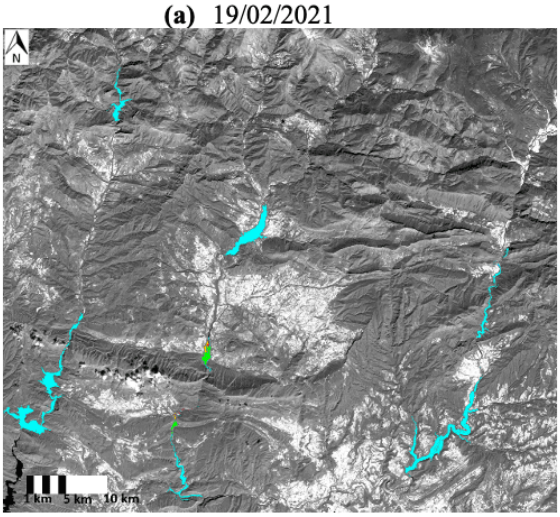

(c) 05/04/2021

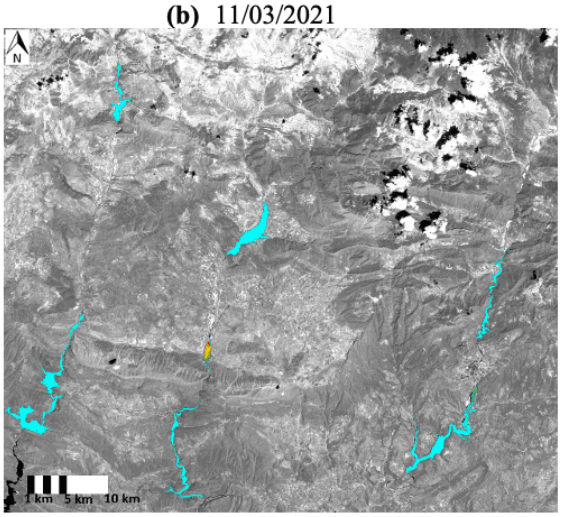

(d) 14/06/2021

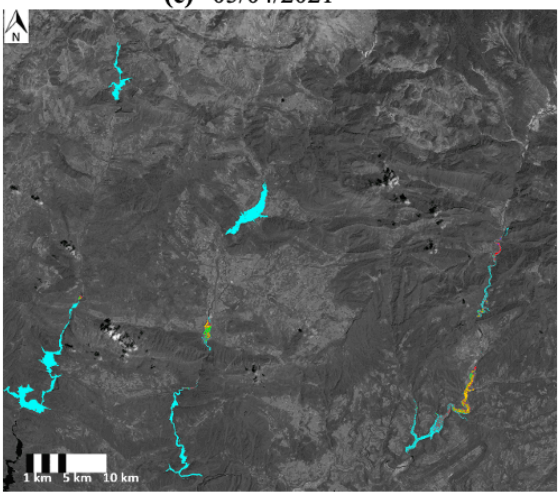

(e) 19/07/21

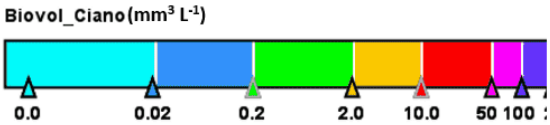

doi.org/10.32388/IEUZZR

Figure B.1. Cyanobacterial biovolume of some Ebro basin reservoirs (Temperate zone). Images from January until July 2021.

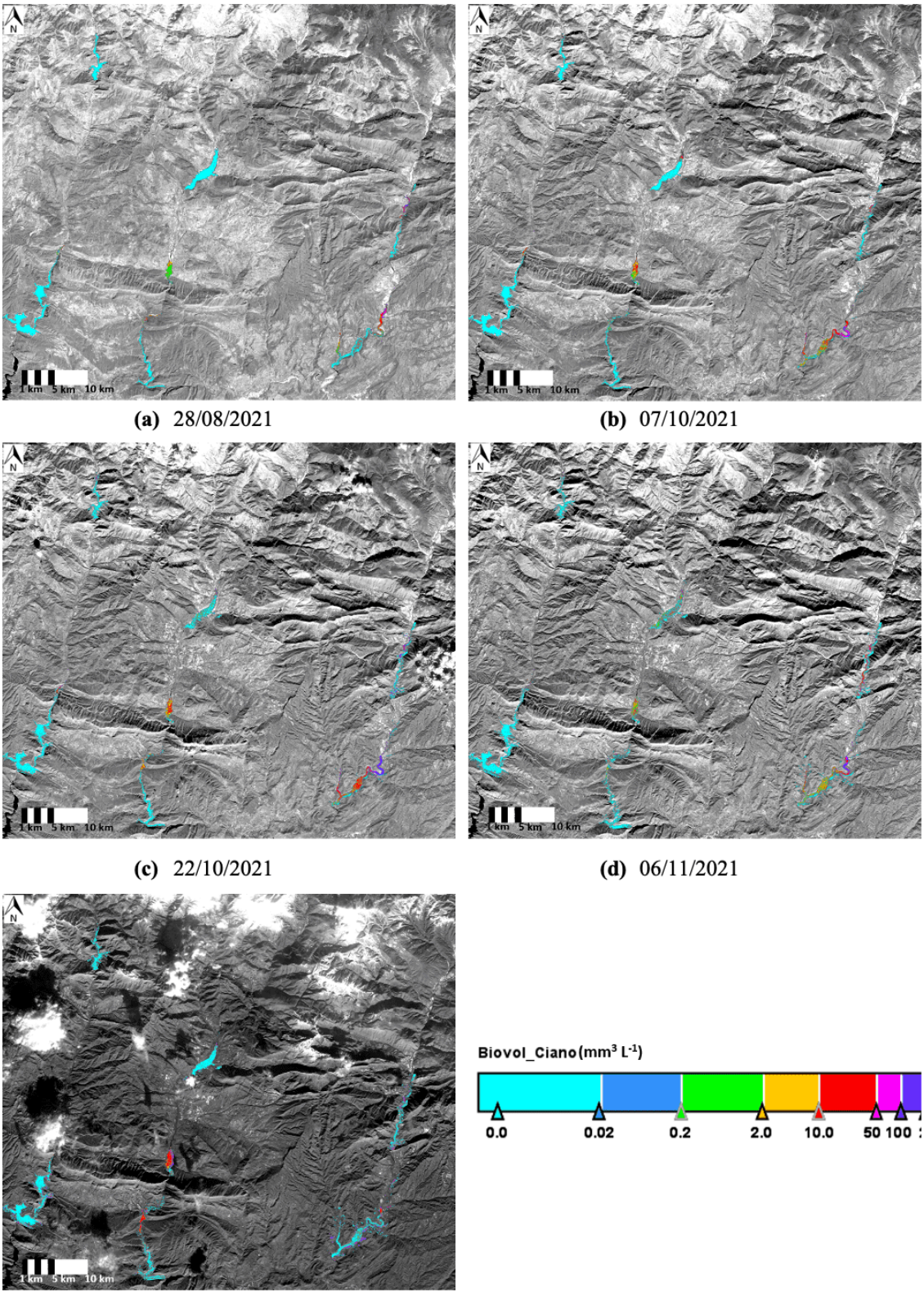

Figure B.2. Cyanobacterial biovolume of some Ebro basin reservoirs (Temperate zone). Images from August until

doi.org/10.32388/IEUZZR

December 2021.

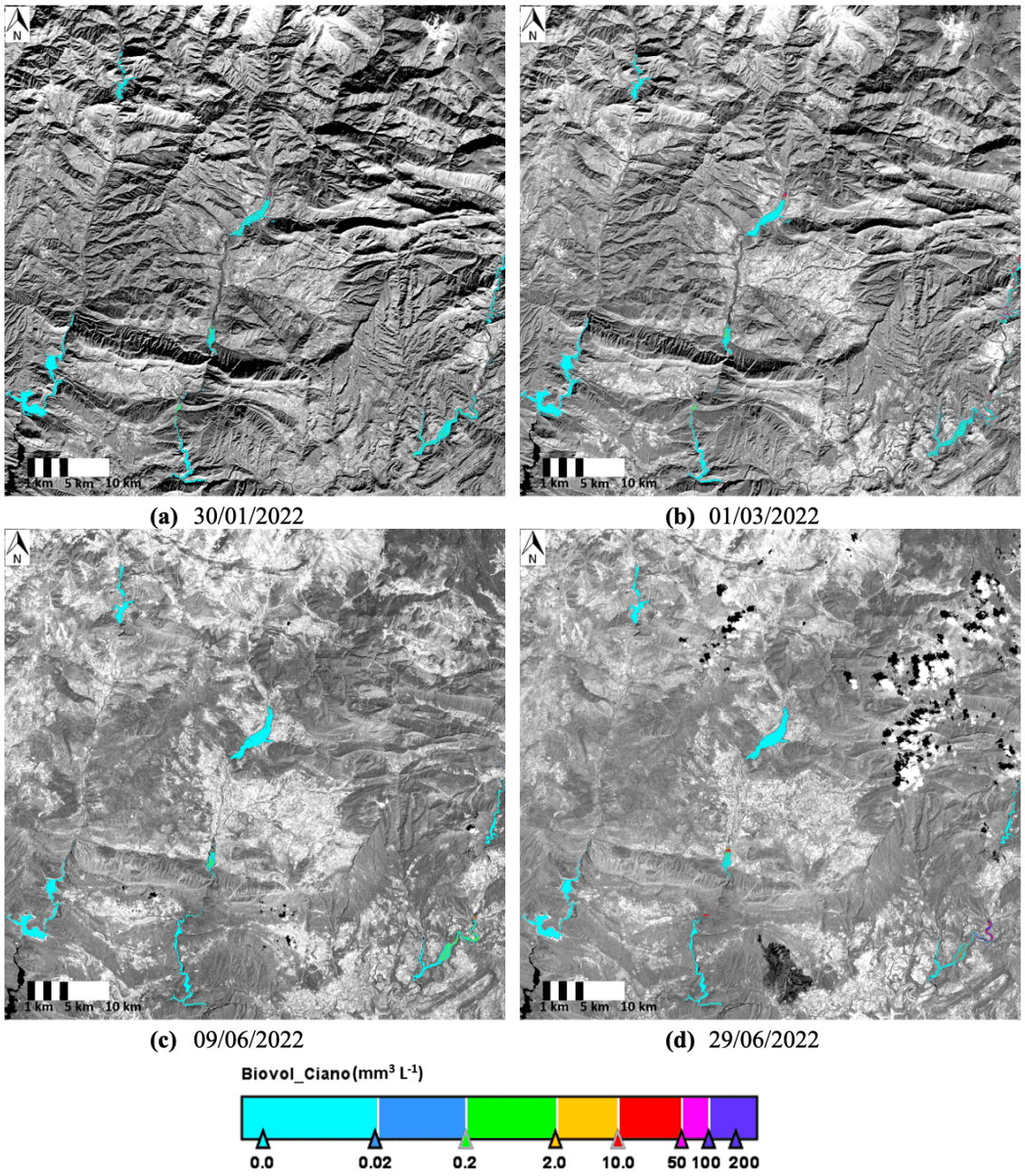

Figure B.3. Cyanobacterial biovolume of some Ebro basin reservoirs (Temperate zone). Images from January until June 2022.

doi.org/10.32388/IEUZZR

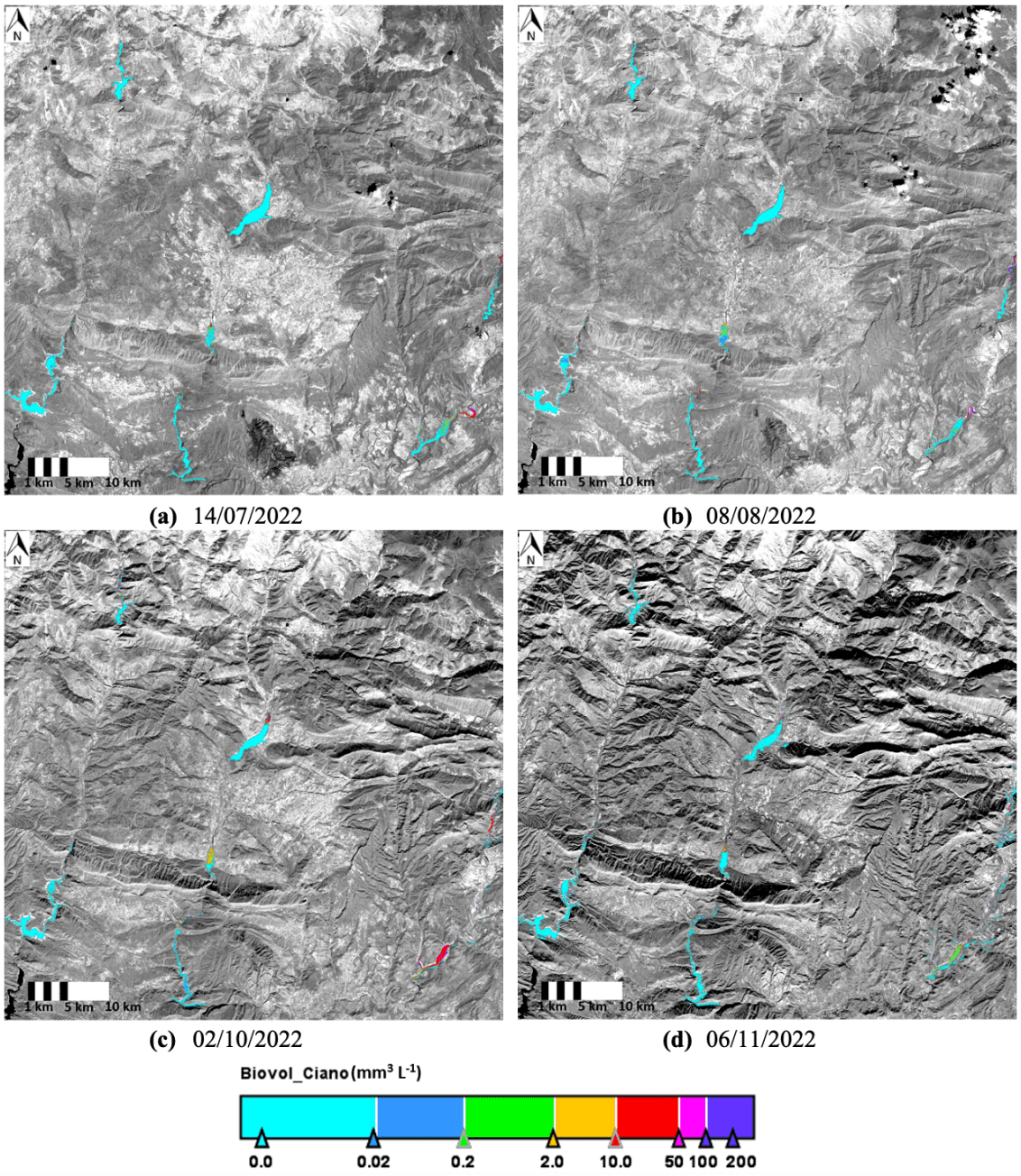

Figure B.4. Cyanobacterial biovolume of some Ebro basin reservoirs (Temperate zone). Images from July until November 2022.

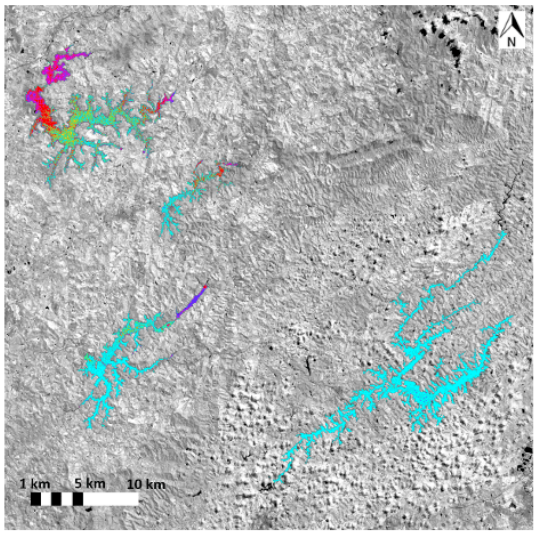

(a) 27/03/2021

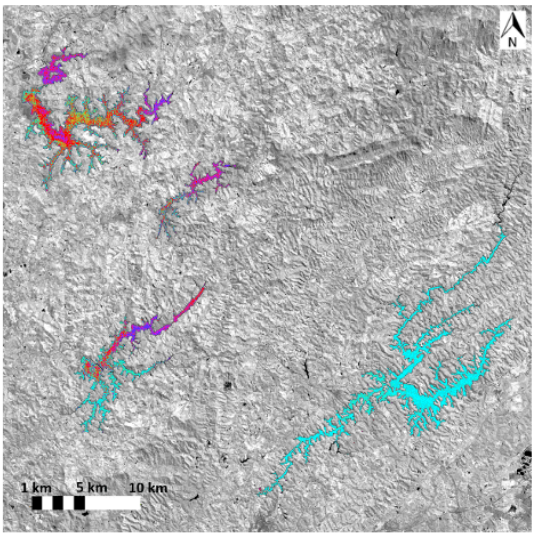

(b) 11/04/2021

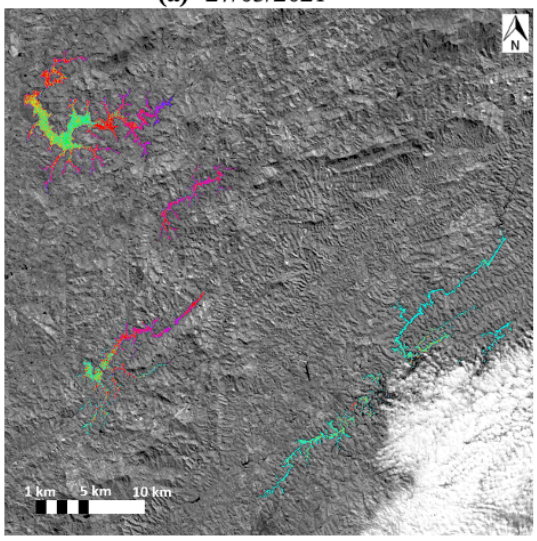

(c) 26/05/2021

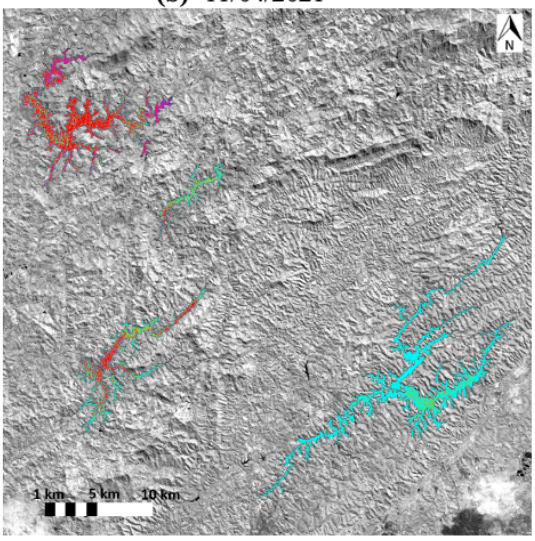

(d) 25/06/2021

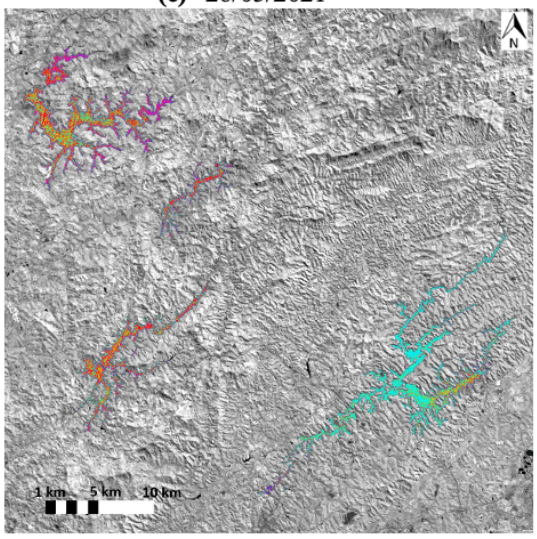

(e) 25/07/21

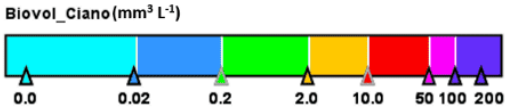

doi.org/10.32388/IEUZZR

Figure B.5. Cyanobacterial biovolume of some Tietê basin reservoirs (Subtropical zone). Images from January until July 2021.

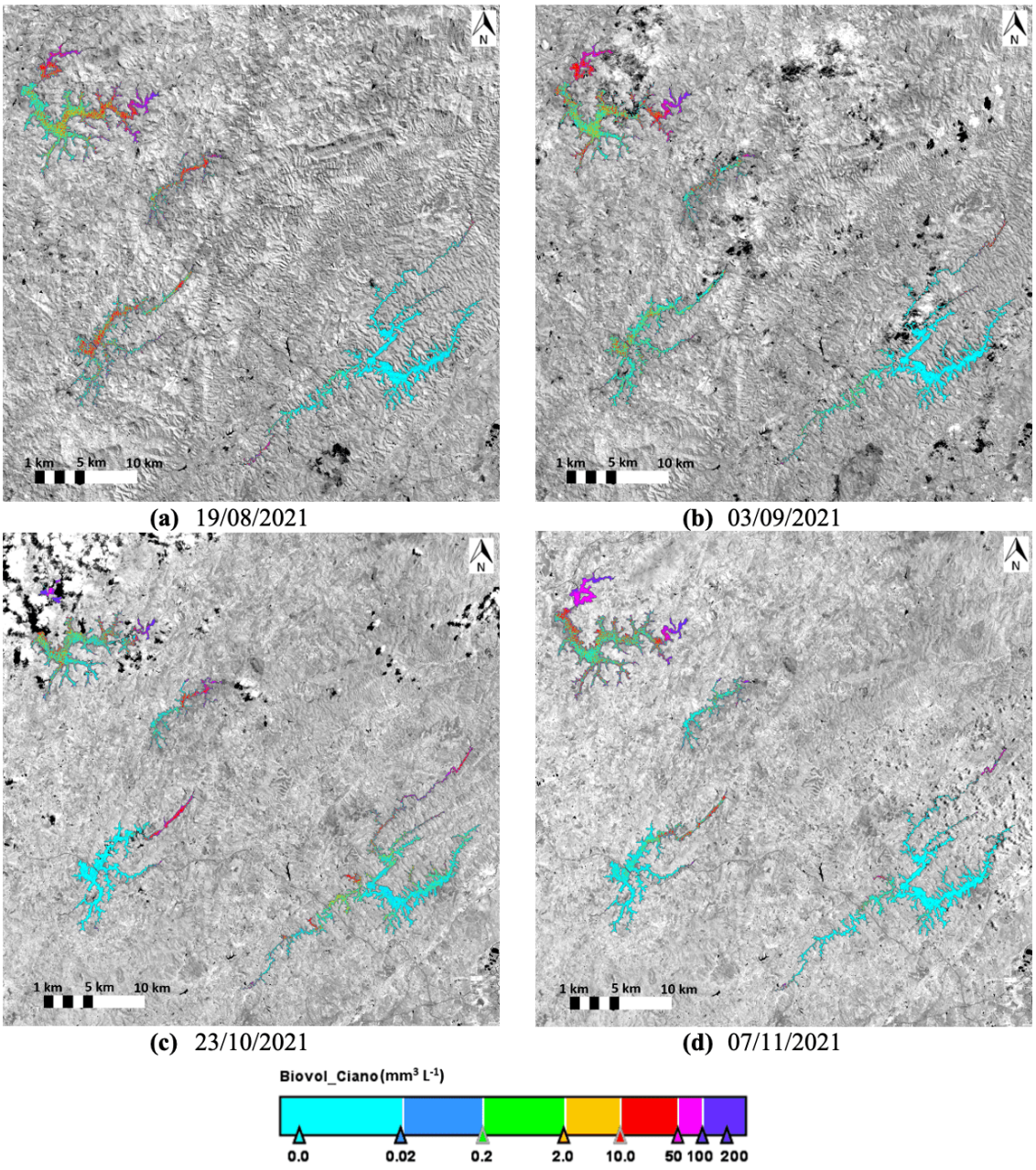

Figure B.6. Cyanobacterial biovolume of some Tietê basin reservoirs (Subtropical zone). Images from August until December 2021.

doi.org/10.32388/IEUZZR

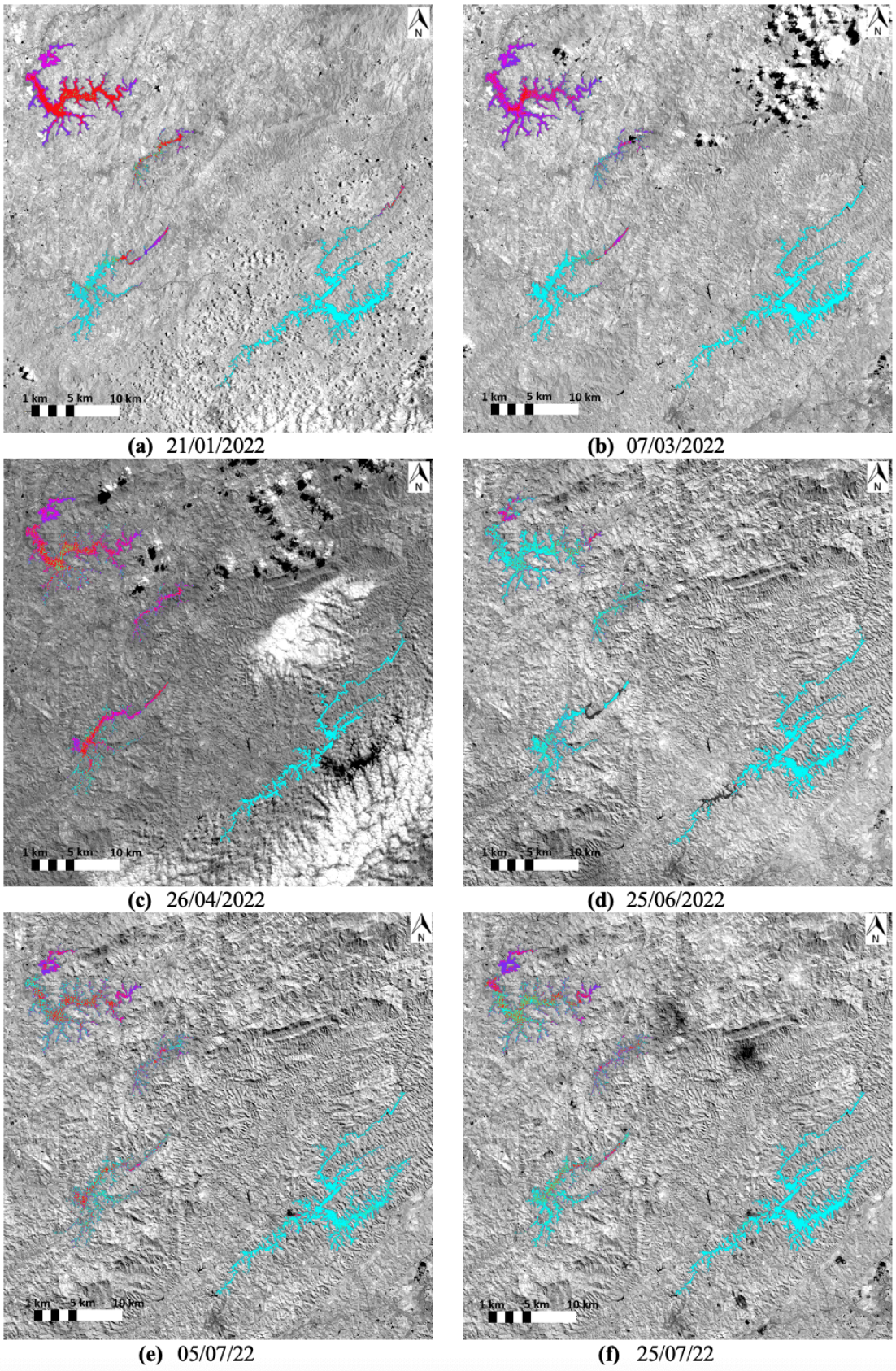

(a) 21/01/2022 (b) 07/03/2022

(c) 26/04/2022 (d) 25/06/2022

(e) 05/07/22 (f) 25/07/22

doi.org/10.32388/IEUZZR

Figure B.7. Cyanobacterial biovolume of some Tietê basin reservoirs (Subtropical zone). Images from January until July 2022.

doi.org/10.32388/IEUZZR

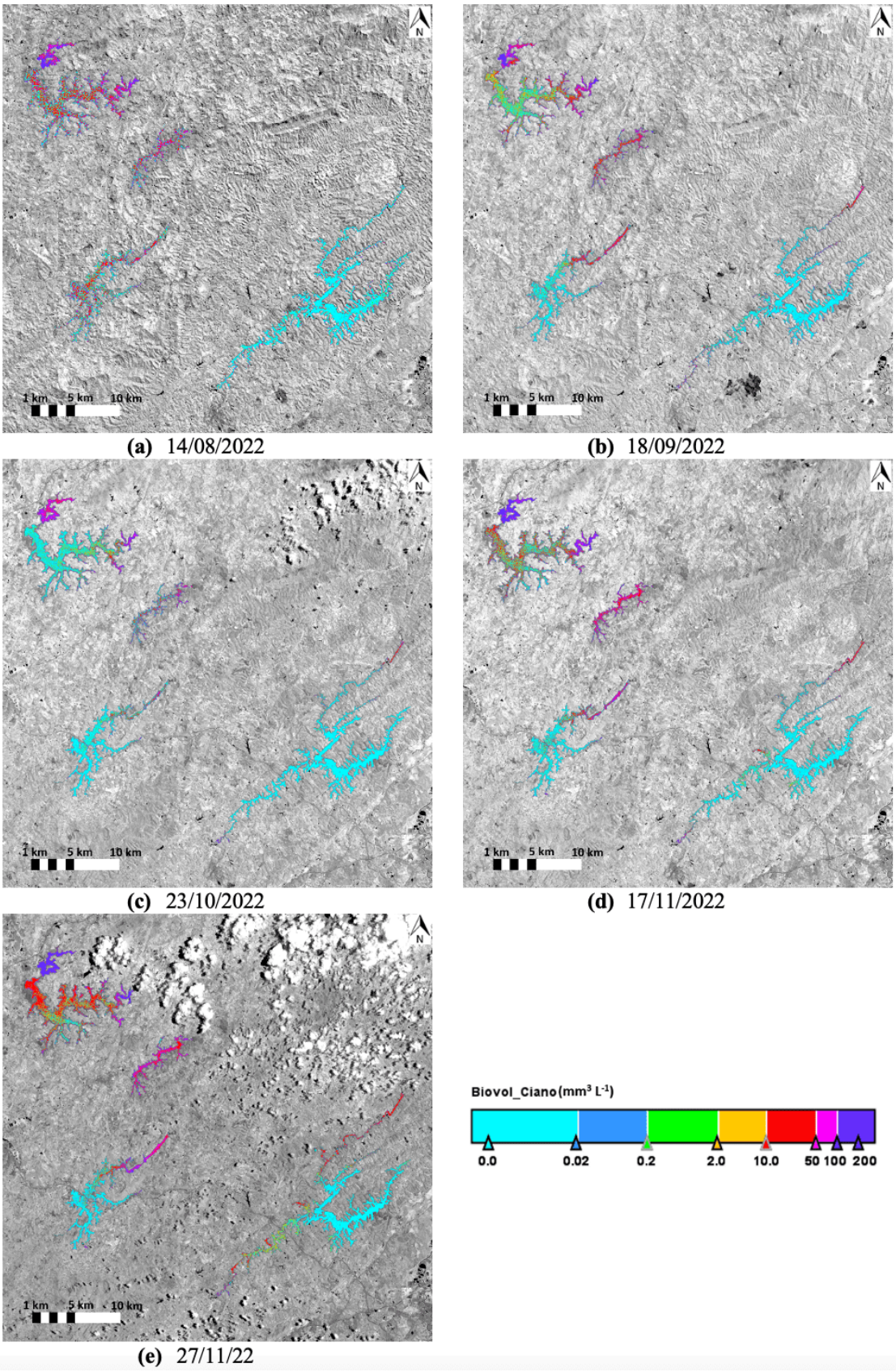

(a) 14/08/2022 **(b)** 18/09/2022

(c) 23/10/2022 **(d)** 17/11/2022

(e) 27/11/22

Figure B.8. Cyanobacterial biovolume of some Tietê basin reservoirs (Subtropical zone). Images from August until November 2022.

Statements and Declarations

Funding

This research was partially funded by the projects regarding the monitoring and control of heavily modified water bodies studies accomplished by the Ebro Basin Authority (Spanish Government) to E. Vicente, the project SEQUARMON (Sentinel quality reservoirs monitoring), APOSTD/2020/134 by Generalitat Valenciana and the European Social Fund postdoc research grant to X. Sòria-Perpinyà, and the project FAPESP 2019/10845-4 granted to M. Pompêo.

Potential Competing Interests

The authors declare no competing interests.

Ethics

Not applicable.

Consent to Participate

Not applicable.

Consent to Publish

All authors agreed to publish the work.

Data Availability

Data will be made available on request.

Author Contributions

All authors contributed to the design of this study. The conceptualization was made by José Moreno, Eduardo Vicente and Marcelo Pompêo. The methodology was designed by Xavier Sòria-Perpinyà and Jesús Delegido. The samples analysis and data curation were performed by Maria Dolores Sendra and Viviane Moschini-Carlos. Image processing and validation were achieved by Rebeca Pérez-González, Patricia Urrego and Juan Miguel Soria. The first

draft of the manuscript was written by Xavier Sòria-Perpinyà and all authors commented on previous versions of the manuscript. All authors read and approved the final manuscript.

References

1. ^*Whitton BA (ed) (2012). Introduction to the Cyanobacteria. Ecology of Cyanobacteria II: Their Diversity in Space and Time. Dordrecht: Springer.*
2. ^*Kasinak JME, Holt BM, Chislock MF, Wilson AE (2015). "Benchtop Fluorometry of Phycocyanin as a Rapid Approach fo r Estimating Cyanobacterial Biovolume." J Plankton Res. **37**(1):248–257. doi:10.1093/plankt/fbu096.*
3. ^*Paerl HW, Havens KE, Hall NS, Otten TG, Zhu M, Xu H, Zhu G, Qin B (2019). "Mitigating a Global Expansion of Toxic Cy anobacterial Blooms: Confounding Effects and Challenges Posed by Climate Change." Mar Fresh Res. **71**(5):579–592. d oi:10.1071/MF18392.*
4. ^*Lunetta RS, Shao Y, Ediriwickrema J, Lyon JG (2010). "Monitoring Agricultural Cropping Patterns Across the Laurentia n Great Lakes Basin Using MODIS-NDVI Data." Int J Appl Earth Obs Geoinf. **12**(2):81–88. doi:10.1016/j.jag.2009.11.005.*
5. ^*Lee TA, Rollwagen-Bollens G, Bollens SM (2015). "The Influence of Water Quality Variables on Cyanobacterial Blooms and Phytoplankton Community Composition in a Shallow Temperate Lake." Environ Monit Assess. **187**(6):315. doi:10.10 07/s10661-015-4550-2.*
6. ^*Schindler DW (1977). "Evolution of Phosphorus Limitation in Lakes." Science. **195**:260–262.*
7. ^*Antenucci JP, Ghadouani A, Burford MA, Romero JR (2005). "The Long-Term Effect of Artificial Destratification on Ph ytoplankton Species Composition in a Subtropical Reservoir." Freshw Biol. **50**(6):1081–1093. doi:10.1111/j.1365-2427.2005. 01374.x.*
8. a, b*Reynolds CS, Huszar V, Kruk C, Naselli-Flores L, Melo S (2021). "Towards a Functional Classification of the Freshwat er Phytoplankton." J Plankton Res. **24**(5):417–428. doi:10.1093/plankt/24.5.417.*
9. a, b*Donis D, Mantzouki E, McGinnis DF, Vachon D, Gallego I, Grossart HP, Rodríguez V (2021). "Stratification Strength an d Light Climate Explain Variation in Chlorophyll A at the Continental Scale in a European Multilake Survey in a Heatw ave Summer." Limnol Oceanogr. **66**(12):4314–4333. doi:10.1002/lno.11963.*
10. ^*Paerl HW, Huisman J (2009). "Climate Change: A Catalyst for Global Expansion of Harmful Cyanobacterial Blooms." Environ Microbiol Rep. **1**(1):27–37. doi:10.1111/j.1758-2229.2008.00004.x.*
11. ^*Mantzouki E, Lürling M, Fastner J, de Senerpont Domis L, Wilk-Woźniak E, Koreivienė J, Warming TP (2018). "Temper ature Effects Explain Continental Scale Distribution of Cyanobacterial Toxins." Toxins. **10**(4):156. doi:10.3390/toxins100 40156.*
12. a, b*Wagner C, Adrian R (2009). "Cyanobacteria Dominance: Quantifying the Effects of Climate Change." Limnol Ocean ogr. **54**(6part2):2460–2468. doi:10.4319/lo.2009.54.6_part_2.2460.*

13. ^Riddick CAL, Hunter PD, Domínguez Gómez JA, Martinez-Vicente V, Présing M, Horváth H, Kovács AW, Vörös L, Zsigmond E, Tyler AN (2019). "Optimal Cyanobacterial Pigment Retrieval from Ocean Colour Sensors in a Highly Turbid, Optically Complex Lake." Remote Sens. **11**(13):1613. doi:10.3390/rs11131613.
14. a, bThomson-Laing G, Puddick J, Wood SA (2020). "Predicting Cyanobacterial Biovolumes from Phycocyanin Fluorescence Using a Handheld Fluorometer in the Field." Harmful Algae. **97**:101869. doi:10.1016/j.hal.2020.101869.
15. a, b, c, dChorus I, Welker M (eds) (2021). Toxic Cyanobacteria in Water. 2nd ed. London: CRC Press.
16. a, bChorus I, Bartram J (eds) (1999). Toxic Cyanobacteria in Water. A Guide to Their Public Health Consequences, Monitoring and Management. London: E&FN Spon.
17. ^Huisman J, Hulot FD (2005). "Population Dynamics of Harmful Cyanobacteria." In: Huisman J, Matthijs HC, Visser PM (eds) Harmful Cyanobacteria. Dordrecht: Springer, pp 143–176. doi:10.1007/1-4020-3022-3 7.
18. a, b, cLunetta RS, Schaeffer BA, Stumpf RP, Keith D, Jacobs SA, Murphy MS (2015). "Evaluation of Cyanobacteria Cell Count Detection Derived from MERIS Imagery Across the Eastern USA." Remote Sens Environ. **157**:24–34. doi:10.1016/j.rse.2014.06.008.
19. ^Backer LC (2002). "Cyanobacterial Harmful Algal Blooms (CyanoHABs): Developing a Public Health Response." Lake Reserv Manag. **18**(1):20–31. doi:10.1080/07438140209353926.
20. ^Dodds WK, Bouska WW, Eitzmann JL, Pilger TJ, Pitts KL, Riley AJ, Schloesser JT, Thornbrugh DJ (2009). "Eutrophication of U.S. Freshwaters: Analysis of Potential Economic Damages." Environ Sci Technol. **43**(1):12–19. doi:10.1021/es801217q.
21. ^Steffensen DA (2008). "Economic Cost of Cyanobacterial Blooms." In: Hudnell HK (ed) Cyanobacterial Harmful Algal Blooms: State of the Science and Research Needs. New York: Springer, pp 855–865.
22. ^Humpage A, Cuniliffe D (2021). "Exposure to Cyanotoxins: Understanding It and Short-Term Interventions to Prevent It. Drinking-Water." In: Chorus I, Welker M (eds) Toxic Cyanobacteria in Water. 2nd edn. London: CRC Press, pp 305–332.
23. ^Williamson N, Kobayashi T, Outhet D, Bowling LC (2018). "Survival of Cyanobacteria in Rivers Following Their Release in Water from Large Headwater Reservoirs." Harmful Algae. **75**:1–15. doi:10.1016/j.hal.2018.04.004.
24. ^Amorim CA, Dantas EW, Moura AN (2020). "Modeling Cyanobacterial Blooms in Tropical Reservoirs: The Role of Physicochemical Variables and Trophic Interactions." Sci Total Environ. **744**:140659. doi:10.1016/j.scitotenv.2020.140659.
25. ^Sobiechowska-Sasim M, Ston-Egiert J, Kosakowska A (2014). "Quantitative Analysis of Extracted Phycobilin Pigments in Cyanobacteria—An Assessment of Spectrophotometric and Spectrofluorometric Methods." J Appl Phycol. **26**(5):2065–2074. doi:10.1007/s10811-014-0244-3.
26. ^Park YJ, Ruddick K (2010). "Detection of Algal Blooms in European Waters Based on Satellite Chlorophyll Data from MERIS and MODIS." Int J Rem Sens. **31**(24):6567–6583. doi:10.1080/01431161003801369.
27. ^Richardson L (1996). "Remote Sensing of Algal Bloom Dynamics." BioScience. **46**:492–501. https://www.jstor.org/stable/1312927.
28. ^Almuhtaram H, Kibuye FA, Ajjampur S, Glover CM, Hofmann R, Gaget V, Owen C, Wert EC, Zamyadi A (2021). "State of Knowledge on Early Warning Tools for Cyanobacteria Detection." Ecol Indic. **133**:108442. doi:10.1016/j.ecolind.2021.1084

42.

29. a, b, c, d, eSòria-Perpinyà X, Vicente E, Urrego P, Pereira-Sandoval M, Tenjo C, Ruíz-Verdú A, Delegido J, Soria JM, Peña R, Moreno J (2021). "Validation of Water Quality Monitoring Algorithms for Sentinel-2 and Sentinel-3 in Mediterranean In land Waters with In Situ Reflectance Data." Water. **13**(5):686. doi:10.3390/w13050686.

30. a, bSun J, Liu D (2003). "Geometric Models for Calculating Cell Biovolume and Surface Area for Phytoplankton." J Plankt on Res. **25**(11):1331–1346. doi:10.1093/plankt/fbg096.

31. ^Verity PG, Robertson C, Tronzo CR, Andrews MG, Nelson JR, Sieracki ME (1992). "Relationships Between Cell Volume a nd the Carbon and Nitrogen Content of Marine Photosynthetic Nanoplankton." Limnol Oceanogr. **37**:1434–46.

32. ^Felip M, Catalan J (2000). "The Relationship Between Phytoplankton Biovolume and Chlorophyll in a Deep Oligotrop hic Lake: Decoupling in Their Spatial and Temporal Maxima." J Plankton Res. **22**:91–105.

33. a, b, c, dMedina-Cobo M, Domínguez JA, Quesada A, De Hoyos C (2014). "Estimation of Cyanobacteria Biovolume in Wat er Reservoirs by MERIS Sensor." Water Res. **63**:10–20. doi:10.1016/j.watres.2014.06.001.

34. ^Hunter PD, Tyler AN, Carvalho L, Codd GA, Maberly SC (2010). "Hyperspectral Remote Sensing of Cyanobacterial Pig ments as Indicators for Cell Populations and Toxins in Eutrophic Lakes." Remote Sens Environ. **114**(11):2705–2718. doi:1 0.1016/j.rse.2010.06.006.

35. ^Wynne TT, Stumpf RP, Tomlinson MC, Dybleb J (2010). "Characterizing a Cyanobacterial Bloom in Western Lake Erie Using Satellite Imagery and Meteorological Data." Limnol Oceanogr. **55**(5):2025–2036. doi:10.4319/lo.2010.55.5.2025.

36. a, b, c, dIsenstein EM, Trescott A, Park MH (2014). "Multispectral Remote Sensing of Harmful Algal Blooms in Lake Cha mplain, USA." Water Environ Res. **86**(12):2271–2278. doi:10.2175/106143014X13975035526149.

37. a, bJohansen RA, Reif MK, Saltus CL, Pokrzywinski KL (2022). "A Review of Empirical Algorithms for the Detection and Quantification of Harmful Algal Blooms Using Satellite-Borne Remote Sensing." U.S. Army Engineer Research and Dev elopment Center, Aquatic Nuisance Species Research Program.

38. ^Kutser T, Paavel B, Verpoorter C, Ligi M, Soomets T, Toming K, Casal G (2016). "Remote Sensing of Black Lakes and Usi ng 810 Nm Reflectance Peak for Retrieving Water Quality Parameters of Optically Complex Waters." Remote Sens. **8**(6): 497. doi:10.3390/rs8060497.

39. a, bOgashawara I, Kiel C, Jechow A, Kohnert K, Ruhtz T, Grossart HP, Wollrab S (2021). "The Use of Sentinel-2 for Chlorop hyll-A Spatial Dynamics Assessment: A Comparative Study on Different Lakes in Northern Germany." Remote Sens. **13**:1 542.

40. ^Bresciani M, Pinardi M, Free G, Luciani G, Ghebrehiwot S, Laanen M, Giardino C (2020). "The Use of Multisource Optic al Sensors to Study Phytoplankton Spatio-Temporal Variation in a Shallow Turbid Lake." Water. **12**:284.

41. ^Tuygun GT, Salgut S, Elçi A (2023). "Long-Term Spatial-Temporal Monitoring of Eutrophication in Lake Burdur Using Remote Sensing Data." Water Sci Technol. **87**:2184–2194.

42. ^Vicente E, Hoyos C, Sánchez P, Cambra J (2005). "Metodología para el Establecimiento el Estado Ecológico Según la Di rectiva Marco del Agua. Protocolos de Muestreo y Análisis para Fitoplancton" [Methodology for Establishing the Ecolo

gical Status According to the Water Framework Directive. Sampling and Analysis Protocols for Phytoplankton]. Ministe rio de Medio Ambiente, Confederación Hidrográfica del Ebro.

43. ^ a b *Gregor J, Maršálek B (2005). "A Simple In Vivo Fluorescence Method for the Selective Detection and Quantification o f Freshwater Cyanobacteria and Eukaryotic Algae." Acta Hydrochim Hydrobiol. **33**:142–148.*
44. ^ *Rousso BZ, Bertone E, Stewart R, Aguiar A, Chuang A, Hamilton DP, Burford MA (2022). "Chlorophyll and Phycocyani n In-Situ Fluorescence in Mixed Cyanobacterial Species Assemblages: Effects of Morphology, Cell Size and Growth Phas e." Water Res. **212**:118127.*
45. ^ *Rousso BZ, Bertone E, Stewart RA, Rinke K, Hamilton DP (2021). "Light-Induced Fluorescence Quenching Leads to Err ors in Sensor Measurements of Phytoplankton Chlorophyll and Phycocyanin." Water Res. **198**:117133.*
46. ^ *Simis SG, Ruiz-Verdú A, Domínguez-Gómez JA, Peña-Martinez R, PetersSW, Gons HJ (2007). "Influence of Phytoplankt on Pigment Composition on Remote Sensing of Cyanobacterial Biomass." Remote Sens Environ. **106**:414–427.*
47. ^ *Lee T, Tsuzuki M, Takeuchi T, Yokoyama K, Karube I (1994). "In-Vivo Fluorometric Method for Early Detection of Cyan obacterial Waterblooms." J Appl Phycol. **6**:489–495.*
48. ^ *Lee TY, Tsuzuki M, Takeuchi T, Yokoyama K, Karube I (1995). "Quantitative-Determination of Cyanobacteria in Mixed Phytoplankton Assemblages by an In-Vivo Fluorometric Method." Anal Chim Acta. **302**:81–87.*
49. ^ *Asai R, Horiguchi Y, Yoshida A, McNiven S, Tahira P, Ikebukuro K, et al (2001). "Detection of Phycobilin Pigments and T heir Seasonal Change in Lake Kasumigaura Using a Sensitive In Situ Fluorometric Sensor." Anal Lett. **34**:2521–2533.*
50. ^ *Izydorczyk K, Tarczynska M, Jurczak T, Mrowczynski J, Zalewski M (2005). "Measurement of Phycocyanin Fluorescen ce as an Online Early Warning System for Cyanobacteria in Reservoir Intake Water." Environ Toxicol. **20**:425–430.*
51. ^ a b c d *Pérez-González R, Sòria-Perpinyà X, Soria JM, Delegido J, Urrego P, Sendra MD, Ruíz-Verdú A, Vicente E, Moreno J (2021). "Phycocyanin Monitoring in Some Spanish Water Bodies with Sentinel-2 Imagery." Water. **13**(20):2866. doi:10.3 390/w13202866.*
52. ^ *Shoaf WT, Lium BW (1976). "Improved Extraction of Chlorophyll A and B from Algae Using Dimethyl Sulphoxide." Lim nol Oceanogr. **21**:926–928.*
53. ^ *Jeffrey ST, Humphrey GF (1975). "New Spectrophotometric Equations for Determining Chlorophylls A, B, C1 and C2 in Higher Plants, Algae and Natural Phytoplankton." Biochem Physiol Pflanz. **167**:191–194.*
54. ^ *Utermöhl H (1958). "Zur Vervollkommnung der Quantitativen Phytoplankton-Methodik: Mit 1 Tabelle und 15 Abbildu ngen im Text und auf 1 Tafel" [On the Improvement of Quantitative Phytoplankton Methodology: With 1 Table and 15 F igures in the Text and on 1 Plate]. Int Ver Theor Angew Limnol [International Association of Theoretical and Applied Li mnology]. **9**(1):1–38. doi:10.1080/05384680.1958.11904091.*
55. ^ *Hillebrand H, Dürselen CD, Kirschtel D, Pollingher U, Zohary T (1999). "Biovolume Calculation for Pelagic and Benthic Microalgae." J Phycol. **35**(2):403–424. doi:10.1046/J.1529-8817.1999.3520403.X.*
56. ^ *Fonseca BM, Ferragut C, Tucci A, Crossetti LO, Ferrari F, de Campos Bicudo D, de Mattos Bicudo CE (2014). "Biovolume de Cianobactérias e Algas de Reservatórios Tropicais do Brasil com Diferentes Estados Tróficos" [Biovolume of Cyanob*

acteria and Algae from Tropical Reservoirs in Brazil with Different Trophic States]. Hoehnea. ***41****(1):9–30. doi:10.1590/S2236-89062014000100002.*

57. ^a ^b*Fletcher K (ed) (2012). Sentinel-2: ESA's Optical High-Resolution Mission for GMES Operational Services. Noordwijk: ESA Communications. doi:10.1016/j.rse.2011.11.026.*

58. ^a ^b ^c ^d*Sòria-Perpinyà X, Vicente E, Urrego P, Pereira-Sandoval M, Ruíz-Verdú A, Delegido J, Soria JM, Moreno J (2020). "Remote Sensing of Cyanobacterial Blooms in a Hypertrophic Lagoon (Albufera of València, Eastern Iberian Peninsula) Using Multitemporal Sentinel-2 Images." Sci Total Environ.* ***698****:134305. doi:10.1016/j.scitotenv.2019.134305.*

59. ^*Brockmann C, Doerffer R, Peters M, Stelzer K, Embacher S, Ruescas A (2016). "Evolution of the C2RCC Neural Network for Sentinel 2 and 3 for the Retrieval of Ocean Colour Products in Normal and Extreme Optically Complex Waters." In Proceedings of the Living Planet Symposium, Prague, Czech Republic, 9–13 May 2016.*

60. ^*Gitelson AA, Gritz Y, Merzlyak MN (2003). "Relationships Between Leaf Chlorophyll Content and Spectral Reflectance and Algorithms for Non-Destructive Chlorophyll Assessment in Higher Plant Leaves." J Plant Physiol.* ***160****:271–282.*

61. ^*Moses WJ, Saprygin V, Gerasyuk V, Povazhnyy V, Berdnikov S, Gitelson AA (2019). "OLCI-Based NIR-Red Models for Estimating Chlorophyll-A Concentration in Productive Coastal Waters—A Preliminary Evaluation." Environ Res Commun.* ***1****:011002.*

62. ^*Pereira-Sandoval M, Urrego P, Ruiz-Verdú A, Tenjo C, Delegido J, Soria-Perpinyà X, Vicente E, Soria J, Moreno J (2019). "Calibration and Validation of Algorithms for the Estimation of Chlorophyll-A Concentration and Secchi Depth in Inland Waters with Sentinel-2." Limnetica.* ***38****:471–487.*

63. ^*Pahlevan N, Mangin A, Balasubramanian SV, Smith B, Alikas K, Arai K, Barbosa C, Bélanger S, Binding C, Bresciani M, et al (2021). "ACIX-Aqua: A Global Assessment of Atmospheric Correction Methods for Landsat-8 and Sentinel-2 Over Lakes, Rivers, and Coastal Waters." Remote Sens Environ.* ***258****:112366.*

64. ^*Tavares MH, Lins RC, Harmel T, Fragoso CR, Martínez JM, Motta-Marques D (2021). "Atmospheric and Sunglint Correction for Retrieving Chlorophyll-A in a Productive Tropical Estuarine-Lagoon System Using Sentinel-2 MSI Imagery." ISPRS J Photogramm Remote Sens.* ***174****:215–236.*

65. ^*Sòria-Perpinyà X, Delegido J, Urreg EP, Ruíz-Verdú A, Soria JM, Vicente E, Moreno J (2022). "Assessment of Sentinel-2-MSI Atmospheric Correction Processors and In Situ Spectrometry Waters Quality Algorithms." Remote Sens.* ***14****:4794.*

66. ^a ^b*Matthews MW (2011). "A Current Review of Empirical Procedures of Remote Sensing in Inland and Near-Coastal Transitional Waters." Int J Remote Sens.* ***32****(21):6855–6899. doi:10.1080/01431161.2010.512947.*

67. ^a ^b*Viso-Vázquez M, Acuña-Alonso C, Rodríguez JL, Álvarez X (2021). "Remote Detection of Cyanobacterial Blooms and Chlorophyll-A Analysis in a Eutrophic Reservoir Using Sentinel-2." Sustainability.* ***13****(15):8570. doi:10.3390/su13158570.*

68. ^*Morel A, Prieur L (1977). "Analysis of Variation in Ocean Color." Limnol Oceanogr.* ***22****(4):709–722. doi:10.4319/lo.1977.22.4.0709.*

69. ^a ^b ^c*Gitelson A, Schalles J, Rundquist D, Schiebe F, Yacobi Y (1999). "Comparative Reflectance Properties of Algal Cultures with Manipulated Densities." J Appl Phycol.* ***11****(4):345–354. doi:10.1023/A:1008143902418.*

70. ^Dall'Olmo G, Gitelson A, Rundquist D (2003). "Towards a Unified Approach for Remote Estimation of Chlorophyll-A in Both Terrestrial Vegetation and Turbid Productive Waters." Geophys Res Lett. **30**:1938.

71. ^Sòria-Perpinyà X, Urrego P, Pereira-Sandoval M, Ruiz-Verdú A, Peña R, Soria JM, Delegido J, Vicente E, Moreno J (2019). "Monitoring the Ecological State of a Hypertrophic Lake (Albufera of València, Spain) Using Multitemporal Sentinel-2 I mages." Limnetica. **38**:457–469.

72. ^Cairo C, Barbosa C, Lobo F, Novo E, Carlos F, Maciel D, Flores RJr, Silva E, Curtarelli V (2019). "Hybrid Chlorophyll-A Alg orithm for Assessing Trophic States of a Tropical Brazilian Reservoir Based on MSI/Sentinel-2 Data." Remote Sens. **12**:4 0.

73. a, b, cMishra S, Mishra DR (2012). "Normalized Difference Chlorophyll Index: A Novel Model for Remote Estimation of C hlorophyll-A Concentration in Turbid Productive Waters." Remote Sens Environ. **117**:394–406.

74. ^Caballero I, Fernández R, Escalante OM, Mamán L, Navarro G (2020). "New Capabilities of Sentinel-2A/B Satellites Co mbined with In Situ Data for Monitoring Small Harmful Algal Blooms in Complex Coastal Waters." Sci Rep. **10**:1–14.

75. a, bKhalili MH, Hasanlou M (2019). "Harmful Algal Blooms Monitoring Using SENTINEL-2 Satellite Images." In Proceed ings of GeoSpatial Conference, Karaj, Iran, 12–14 October 2019.

76. a, bCillero Castro C, Domínguez Gómez JA, Delgado Martín J, Hinojo Sánchez BA, Cereijo Arango JL, Cheda Tuya FA, Día z-Varela R (2020). "An UAV and Satellite Multispectral Data Approach to Monitor Water Quality in Small Reservoirs." R emote Sens. **12**:1514.

77. a, b, cWynne TT, Mishra S, Meredith A, Litaker RW, Stumpf RP (2021). "Intercalibration of MERIS, MODIS, and OLCI Satel lite Imagers for Construction of Past, Present, and Future Cyanobacterial Biomass Time Series." Remote Sens. **13**:2305.

78. ^Gitelson A (1992). "The Peak Near 700nm on Radiance Spectra of Algae and Water: Relationships of Its Magnitude an d Position with Chlorophyll Concentration." Int J Remote Sens. **13**:3367–3373.

79. ^Rivera JP, Verrelst J, Delegido J, Veroustraete F, Moreno J (2014). "On the Semi-Automatic Retrieval of Biophysical Para meters Based on Spectral Index Optimization." Remote Sens. **6**:4927–4951.

80. ^Verrelst J, Rivera J, Alonso L, Moreno J (2014). "ARTMO: An Automated Radiative Transfer Models Operator Toolbox for Automated Retrieval of Biophysical Parameters Through Model Inversion." In Proceedings of the EARSeL 7th SIG-Imag ing Spectroscopy Workshop, Edinburgh, UK, April 2011.

81. ^Rivera JP, Verrelst J, Gómez-Dans J, Muñoz-Marí J, Moreno J, Camps-Valls G (2015). "An Emulator Toolbox to Approxim ate Radiative Transfer Models with Statistical Learning." Remote Sens. **7**:9347–9370.

82. ^dos Santos Machado L, Dörr F, Dörr FA, Frascareli D, Melo DS, Gontijo ES, Friese K, Pinto E, Rosa AH, Pompêo MM, Mos chini-Carlos V (2023). "Permanent Occurrence of Raphidiopsis Raciborskii and Cyanotoxins in a Subtropical Reservoir Polluted by Domestic Effluents (Itupararanga Reservoir, São Paulo, Brazil)." Environ Sci Pollut Res. **29**(13):18653–18664. doi:10.1007/s11356-021-16994-6.

83. ^Chen J, Zhu W, Tian YQ, Yu Q, Zheng Y, Huang L (2017). "Remote Estimation of Colored Dissolved Organic Matter and Chlorophyll-A in Lake Huron Using Sentinel-2 Measurements." J Appl Remote Sens. **11**(03):036007. doi:10.1117/1.JRS.11.03

6007.

84. ^*Lins RC, Martinez JM, Motta Marques DD, Cirilo JA, Fragoso CR (2017). "Assessment of Chlorophyll-A Remote Sensing Algorithms in a Productive Tropical Estuarine-Lagoon System." Remote Sens.* ***9****(6):516. doi:10.3390/rs9060516.*
85. ^*Xu M, Liu H, Beck R, Lekki J, Yang B, Shu S, Liu Y, Benko T, Anderson R, Tokars R, et al (2019). "Regionally and Locally A daptive Models for Retrieving Chlorophyll-A Concentration in Inland Waters From Remotely Sensed Multispectral and Hyperspectral Imagery." IEEE Trans Geosci Remote Sens.* ***57****:4758–4774. doi:10.1109/TGRS.2019.2892899.*
86. ^*Matthews MW (2017). "Bio-Optical Modeling of Phytoplankton Chlorophyll-A." In: Mishra DR, Ogashawara I, Gitelson AA (eds) Bio-Optical Modeling and Remote Sensing of Inland Waters. Amsterdam: Elsevier, pp 157–188.*
87. ^*Kelly LT, Reed L, Puddick J, Hawes I, Hicks BJ, Allan MG, Lehmann MK, Wood SA (2023). "Growth Conditions Impact Pa rticulate Absorption and Pigment Concentrations in Two Common Bloom Forming Cyanobacterial Species." Harmful Algae.* ***125****:102432.*
88. ^*Ordoñez SJ (2010). Limnología del Embalse de Sau: Relaciones del Zooplancton, la Clorofila y los Sólidos en Suspensió n con el Clima Lumínico del Agua [Limnology of the Sau Reservoir: Relationships of Zooplankton, Chlorophyll and Sus pended Solids with the Luminous Climate of the Water]. Dissertation, Universitat de Barcelona.*
89. ^*Armengol J, Rodríguez JJ, García JC, Ordoñez J, Marcé R (2009). "La Gestión de los Embalses en Relación a la Calidad d el Agua en Condiciones de Sequía Extrema" [The Management of Reservoirs in Relation to Water Quality Under Extre me Drought Conditions]. Ing Agua [Water Engineering].* ***16****(4):285–294. doi:10.4995/ia.2009.2956.*
90. a, b, c, d*Oliver SL, Ribeiro H (2016). "Water Supply, Climate Change and Health Risk Factors: Example Case of São Paulo —Brazil." In: Filho WL, Azeiteiro UM, Alves F (eds) Climate Change and Health: Improving Resilience and Reducing Ris ks. Cham: Springer, pp 433–447.*
91. ^*Dellamano-Oliveira MJ, Vieira AAH, Rocha O, Colombo V, Sant'Anna CL (2008). "Phytoplankton Taxonomic Compositi on and Temporal Changes in a Tropical Reservoir." Fundam Appl Limnol.* ***171****:27–38. doi:10.1127/1863-9135/2008/0171-0 027.*
92. a, b*Tundisi JG, Matsumura-Tundisi T, Abe DS (2008). "The Ecological Dynamics of Barra Bonita (Tietê River, SP, Brazil) Reservoir: Implications for Its Biodiversity." Braz J Biol.* ***68****:1079–1098.*
93. ^*Reynolds CS (2006). Ecology of Phytoplankton (Ecology, Biodiversity and Conservation). Cambridge: Cambridge Univ ersity Press.*
94. ^*Margalef R (1983). Limnología. Barcelona: Ediciones Omega.*
95. ^*Funari E, Manganelli M, Buratti FM, Testai E (2017). "Cyanobacteria Blooms in Water: Italian Guidelines to Assess and Manage the Risk Associated to Bathing and Recreational Activities." Sci Total Environ.* ***598****:867–880. doi:10.1016/j.scitot env.2017.03.232.*
96. ^*Oyama Y, Fukushima T, Matsushita B, Matsuzaki H, Kamiya K, Kobinata H (2015). "Monitoring Levels of Cyanobacter ial Blooms Using the Visual Cyanobacteria Index (VCI) and Floating Algae Index (FAI)." Int J Appl Earth Obs Geoinf.* ***38****: 335–348. doi:10.1016/j.jag.2015.02.002.*

97. ^Jia T, Zhang X, Dong R (2019). "Long-Term Spatial and Temporal Monitoring of Cyanobacteria Blooms Using MODIS o n Google Earth Engine: A Case Study in Taihu Lake." Remote Sens. **11**(19):2269. doi:10.3390/rs11192269.

Declarations

Funding: This research was partially funded by the projects regarding the monitoring and control of heavily modified water bodies studies accomplished by the Ebro Basin Authority (Spanish Government) to E. Vicente, the project SEQUARMON (Sentinel quality reservoirs monitoring), APOSTD/2020/134 by Generalitat Valenciana and the European Social Fund postdoc research grant to X. Sòria-Perpinyà, and the project FAPESP 2019/10845-4 granted to M. Pompêo.

Potential competing interests: No potential competing interests to declare.